Atmos. Chem. Phys., 12, 7371–7389, 2012
www.atmos-chem-phys.net/12/7371/2012/
doi:10.5194/acp-12-7371-2012

Atmospheric Chemistry and Physics

Analysis of IASI tropospheric O_3 data over the Arctic during POLARCAT campaigns in 2008

M. Pommier[1,*], C. Clerbaux[1,2], K. S. Law[1], G. Ancellet[1], P. Bernath[3], P.-F. Coheur[2], J. Hadji-Lazaro[1], D. Hurtmans[2], P. Nédélec[4], J.-D. Paris[5], F. Ravetta[1], T. B. Ryerson[6], H. Schlager[7], and A. J. Weinheimer[8]

[1]UPMC Univ. Paris 06; Université Versailles St-Quentin; UMR8190, CNRS/INSU, LATMOS-IPSL, Paris, France
[2]Spectroscopie de l'Atmosphère, Chimie Quantique et Photophysique, Université Libre de Bruxelles (ULB), Brussels, Belgium
[3]Department of Chemistry, University of York, Heslington, York, UK
[4]Université de Toulouse, UPS; CNRS, Laboratoire d'Aérologie (LA), Toulouse, France
[5]LSCE/IPSL, CEA-CNRS-UVSQ, Saclay, France
[6]NOAA ESRL Chemical Sciences Division, Boulder, Colorado, USA
[7]DLR, Institut für Physik der Atmosphäre, Oberpfaffenhofen, Germany
[8]NCAR, Boulder, USA
[*]now at: Air Quality Research Division, Science and Technology Branch, Environment Canada, Toronto, Ontario, Canada

Correspondence to: M. Pommier (matthieu.pommier@ec.gc.ca)

Received: 1 December 2011 – Published in Atmos. Chem. Phys. Discuss.: 16 December 2011
Revised: 17 April 2012 – Accepted: 12 July 2012 – Published: 16 August 2012

Abstract. Ozone data retrieved in the Arctic region from infrared radiance spectra recorded by the Infrared Atmospheric Sounding Interferometer (IASI) on board the MetOp-A European satellite are presented. They are compared with in situ and lidar observations obtained during a series of aircraft measurement campaigns as part of the International Polar Year POLARCAT activities in spring and summer 2008. Different air masses were sampled during the campaigns including clean air, polluted plumes originating from anthropogenic sources, forest fire plumes from the three northern continents, and stratospheric-influenced air masses. The comparison between IASI O_3 [0–8 km], [0–12 km] partial columns and profiles with collocated aircraft observations is achieved by taking into account the different sensitivity and geometry of the sounding instruments. A detailed analysis is provided and the agreement is discussed in terms of vertical sensitivity and surface properties at the location of the observations. Overall, IASI O_3 profiles are found to be in relatively good agreement with smoothed in situ and lidar profiles in the free troposphere with differences of less than 40 % (25 % over sea for both seasons) and 10 %, respectively. The correlation between IASI O_3 retrieved partial columns and the smoothed aircraft partial columns is good with DC-8 in situ data in spring over North America ($r = 0.68$), and over Greenland with ATR-42 lidar measurements in summer ($r = 0.67$). Correlations with other data are less significant highlighting the difficulty of IASI to capture precisely the O_3 variability in the Arctic upper troposphere and lower stratosphere (UTLS). This is particularly noted in comparison with the [0–12 km] partial columns. The IASI [0–8 km] partial columns display a low negative bias (by less than 26 % over snow) compared to columns derived from in situ measurements. Despite the relatively high biases of the IASI retrievals in the Arctic UTLS, our analysis shows that IASI can be used to identify, using O_3 / CO ratios, stratospheric intrusions.

1 Introduction

The Arctic is a region that is very sensitive to changes in atmospheric dynamics and composition, and is therefore strongly affected by climate change. This area receives pollution from the Northern Hemisphere continents leading

to a phenomenon called "Arctic Haze" that appears every winter and spring in the lower troposphere (Garrett and Verzella, 2008; Greenaway, 1950; Mitchell, 1957) and impacts atmospheric chemistry. The Arctic troposphere is also influenced by ozone (O_3) pollution transported from mid-latitudes (e.g. Shindell et al., 2008). Tropospheric O_3 plays an important role in the chemical processes occurring in the atmosphere and has a major impact on the climate. It is produced by photochemical oxidation of carbon monoxide (CO), methane (CH_4) and non-methane volatile organic compounds (NMVOCs) in the presence of nitrogen oxides NO_x ($NO + NO_2$). Tropospheric O_3 concentrations have increased as a consequence of human activities, especially from photochemical processing of combustion products (e.g. HTAP, 2010). The environmental impact of O_3 varies with altitude since it can act as an air pollutant (lower troposphere) or an oxidizing agent and a greenhouse gas (middle-to-upper troposphere). Tropospheric O_3 is produced locally near to emission regions or also, during long-range transport to, for example, the Arctic or over the North Atlantic (Real et al., 2007). The other main source of tropospheric O_3 is transport from the stratosphere, so-called STE (stratosphere-troposphere exchange) source, and measurements have already shown a strong influence of stratospheric air masses on O_3 concentrations in the Arctic free troposphere (Dibb et al., 2003). STE is favoured during tropopause folds, which are common in the Arctic (Rao et al., 2004). The main O_3 sinks are chemical destruction and dry deposition at the surface. These sinks depend on the geographical location, season, and altitude, in the case of photochemical destruction. Notably, large-scale deposition occurs in summer and autumn over Siberian forests (Engvall Stjernberg et al., 2012).

In order to elucidate factors governing O_3 abundances in the Arctic troposphere, it is essential to measure the global three-dimensional distributions of tropospheric O_3 and its precursors. Satellite data offer extended observations of O_3 that complement the limited number of in situ measurements in the remote Arctic region and provide an integrated view. Sources of satellite data providing information on tropospheric O_3 include tropospheric partial columns derived from the Global Ozone Monitoring Experiment (GOME) (Liu et al., 2005), or more recently from the Ozone Monitoring Instrument (OMI) (Ziemke et al., 2009) and the Tropospheric Emission Spectrometer (TES) (Boxe et al., 2010). The latter study showed that TES O_3 profiles were positively biased ($< 15\,\%$) in the troposphere and lower stratosphere (from ~ 1000 to 100 hPa) when compared to the ozonesonde data in the Arctic.

The IASI instrument, launched on board the sun synchronous MetOp-A satellite platform on the 19 October 2006 in Baïkonour (Kazakhstan) into a polar orbit, provides a good view of long-range transport, particularly the O_3 distribution in the Arctic. Several studies have previously discussed O_3 distributions from IASI including Boynard et al. (2009) on the global scale, Wespes et al. (2012) and Parrington et al. (2012) over North America, and Zyryanov et al. (2012) over Europe. The aim of this paper is to validate IASI O_3 data over the Arctic by taking advantage of high-quality aircraft data from the recent POLARCAT (Polar Study using Aircraft, Remote Sensing, Surface Measurements and Models, of Climate, Chemistry, Aerosols, and Transport) campaigns and the availability of independent airborne observations.

POLARCAT is an international project involving eighteen countries and including coordinated measurement campaigns, data analysis and modelling in order to study the transport of pollution to the Arctic from anthropogenic sources and boreal forest fires. This project aims to assess the impact of pollution on atmospheric composition and climate change in the Arctic. Dedicated measurement campaigns took place from 18 March to 23 April 2008 (spring campaigns) and from 18 June to 29 July 2008 (summer campaigns) and involved five different aircraft measuring O_3: NOAA WP-3D, NASA DC-8, CNRS ATR-42, DLR Falcon-20 and Russian Antonov-30. POLARCAT aircraft collected data in air masses originating from regions influenced by North American, Asian, European and Siberian emissions. Specifically, the ARCPAC (Aerosol, Radiation, and Cloud Processes affecting Arctic Climate) (Brock et al., 2011) and ARCTAS (Arctic Research of the Composition of the Troposphere from Aircraft and Satellites) (Jacob et al., 2010) missions focused on spring and summer boreal fire emissions with Siberian fires also sampled by YAK-AEROSIB (YAK-Airborne Extensive Regional Observations) (Paris et al., 2009) in summer 2008. North American and Asian pollution was observed downwind over Greenland in summer 2008 as part of POLARCAT-France (Pommier et al., 2010) and POLARCAT-GRACE (POLARCAT-GReenland Aerosol and Chemistry Experiment) (Roiger et al., 2011). POLARCAT-France also observed European and Siberian pollution in spring 2008 from northern Sweden. The seasonal evolution of pollutant transport pathways and Arctic chemical composition can be studied by combining spring and summer data.

In this paper, we provide a detailed evaluation of IASI O_3 data over the Arctic. After a brief description of the IASI instrument, the retrieval algorithm and its performance in the Arctic (Sect. 2), we describe the independent data used for the evaluation (Sect. 3). Section 4 presents the methodology used to validate IASI O_3 products, including the use of ACE-FTS data to build up a climatology above 8 km to complement the aircraft data, as well as collocation criteria and a smoothing convention used for the evaluation with aircraft measurements. In Sect. 5, we present a statistical evaluation of the IASI O_3 measurement profiles and partial columns. This evaluation covers the troposphere and the upper troposphere lower stratosphere (UTLS) as a function of surface type. Conclusions are presented in Sect. 6.

2 Ozone observations from IASI

2.1 Instrument and ozone product

The IASI instrument is a nadir-viewing Fourier Transform Spectrometer (FTS) measuring in the thermal infrared (IR) part of the spectrum, between 645 and 2760 cm^{-1}. It records radiance from the Earth's surface and the atmosphere with a spectral resolution of 0.5 cm^{-1} (apodized), spectrally sampled at 0.25 cm^{-1}, and with a low radiometric noise (better than 0.2 K at 280 K in the O_3 spectral region located around 9.6 µm). The IASI field of view is composed of 2×2 circular pixels each with a ground footprint of 12 km diameter at nadir and it has an across-track scan with a swath width of 2200 km. Due to its spatial coverage, combined with its low radiometric noise, IASI provides twice daily global measurements of key atmospheric species (e.g. CO, O_3, NH_3, CH_3OH, HNO_3) enabling the analysis of local pollution events, global distributions and transport (Clerbaux et al., 2009).

The absorption lines within each spectrum are related to the trace gas concentrations via a non- linear function that involves the surface and atmosphere characteristics at the point of measurement such as surface emissivity, temperature profile and other atmospheric chemical composition, clouds etc. They are also related to the characteristics of the instrument itself (spectral resolution, footprint, radiometric noise). To retrieve information about specific atmospheric trace gases from these spectra, an inversion algorithm/retrieval scheme is required.

For this work, the IASI O_3 distributions are retrieved from IASI radiance spectra using the FORLI-O_3 (Fast Optimal Retrievals on Layers for IASI-O_3) retrieval code (Hurtmans et al., 2012). The scheme is based on the Optimal Estimation Method as described by Rodgers (2000). It provides O_3 profiles on 40 levels, along with the associated averaging kernels (AKs) and error matrices. The AK represents the measure of sensitivity of the retrieved state to the true state. The trace of the AK, called Degrees Of Freedom for the Signal (DOFS), indicates the number of independent pieces of information available from the retrieval and therefore gives an estimate of its vertical sensitivity. Retrievals are performed for scenes with cloud coverage lower than 13 % using the Eumetsat operational level 2 cloud parameters (Clerbaux et al., 2009). The FORLI a priori profile and associated covariance matrix were constructed using the Logan/Labow/McPeters climatological database (McPeters et al., 2007). This O_3 climatology depends on altitude and is based on a monthly compilation of O_3 profiles from the surface to 60 km averaged over 10° latitude bins.

Global measurements of O_3 from IASI have been previously examined by Wespes et al. (2012) during the NASA ARCTAS and NOAA ARCPAC campaigns associated with POLARCAT in 2008. This study showed that IASI observations had a positive relative difference of 20 % in North America and in the Arctic compared to the global MOZART-4 (Model for OZone and Related chemical Tracers) chemistry transport model. Another recent study of the Antarctic ozone hole by Scannell et al. (2012), also using the FORLI-O_3 retrieval algorithm, showed good agreement for different months in 2009 between the IASI and GOME-2 instruments (correlation of 0.97 with an IASI positive bias of 7 %). Comparison between IASI and ozonesondes within the ozone hole gave differences of less than 30 %. A validation of total O_3 columns with ground-based Brewer instruments was provided in Antón et al. (2011) and showed that FORLI-O_3 data were slightly overestimated when compared to the ground-based data ($\sim$ 4.4 %). Inter-comparison of IASI O_3 products using three independent retrieval algorithms with ozonesondes covering the mid-latitudes and the tropics from January to December 2008 showed that all algorithms perform equally well, although they tended to systematically overestimate O_3 concentrations in the UTLS region by 10 % to 25 % (depending on the algorithms) (Dufour et al., 2012). FORLI-O_3 tropospheric columns did not show significant biases compared to the sonde data.

In this work IASI data are filtered out if the root mean square (RMS) of the spectral residuals (difference between the measured and the calculated spectra after the last fitting iteration) exceeds 3.5×10^{-8} W (m^{-2} sr cm^{-1}) and if the bias exceeds 1.25×10^{-9} W (m^2 sr cm^{-1}) or is lower than -0.75×10^{-9} W (m^2 sr cm^{-1}) (Hurtmans et al., 2012). Figure 1 shows global day-time total O_3 columns averaged over a $1° \times 1°$ grid for the periods of the measurement campaigns using this filter. In this study, daytime is defined as the period corresponding to a solar zenith angle (SZA) of 83° or smaller and night-time to a SZA of 90° or larger. Figure 1 highlights the seasonal variability of daytime total O_3 columns in the Arctic with higher O_3 concentrations in spring (mean value above 65° N of $\sim 9.7 \times 10^{18}$ molecules cm^{-2}) (Fig. 1a) compared to summer (mean value above 65° N $\sim 8.6 \times 10^{18}$ molecules cm^{-2}) (Fig. 1b). Figure 2 shows the corresponding number of IASI observations on a $1° \times 1°$ grid. Note in Fig. 2b the high density of observations at high latitudes in the summer period compared to Fig. 2a, showing that most of IASI data used for the validation were provided during the day. Note also that a few gaps exist in spring because MetOp-A was often in calibration mode.

2.2 IASI O_3 performance in the Arctic

The Arctic is a challenging region for the retrieval of tropospheric concentrations using a nadir-viewing thermal-IR instrument (Clerbaux et al., 2009). Due to cold surface temperatures, and low thermal contrast within the first layer of the atmosphere, Arctic retrievals are characterized by low DOFS. Figure 3 shows typical AK functions from FORLI-O_3 retrievals in the Arctic. Three different levels of sensitivity maxima are apparent: [2–6 km], [6–12 km] and [14–20 km]. All rows of the AK matrix influence each altitude

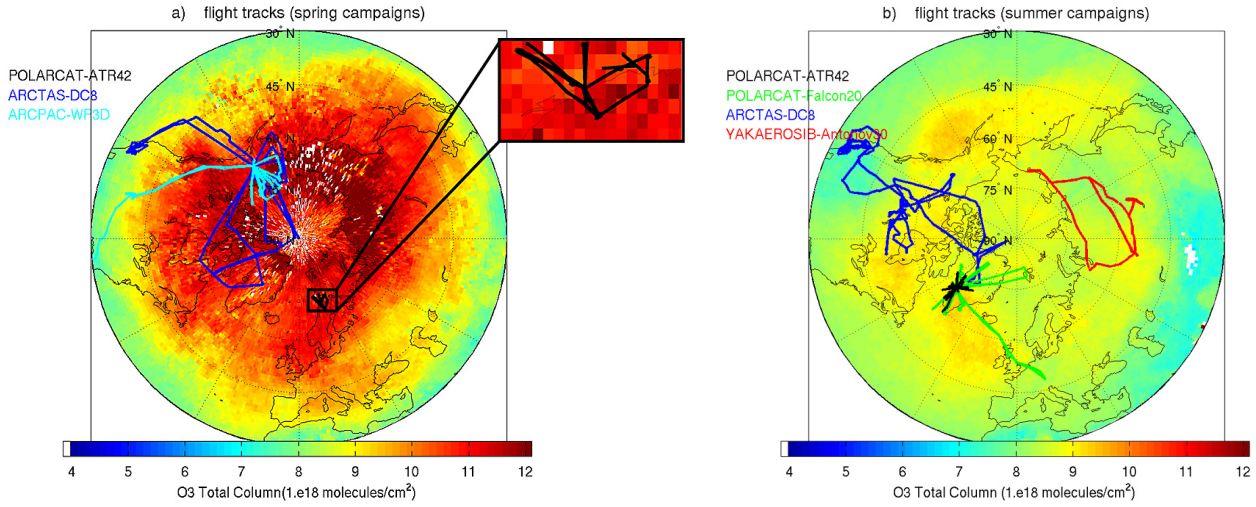

Fig. 1. Global distributions of daytime IASI total O_3 columns averaged from 18 March to 23 April 2008 (period of POLARCAT spring campaigns) with a zoom on ATR-42 flight area **(a)** and for 18 June to 29 July 2008 (period of POLARCAT summer campaigns) **(b)**. IASI data are averaged over a $1° \times 1°$ grid. White areas indicate no data. Flight-tracks for all flights of the DC-8 (blue), ATR-42 (black), WP-3D (cyan), Falcon-20 (green) and Antonov-30 (red) aircraft are superimposed on the maps.

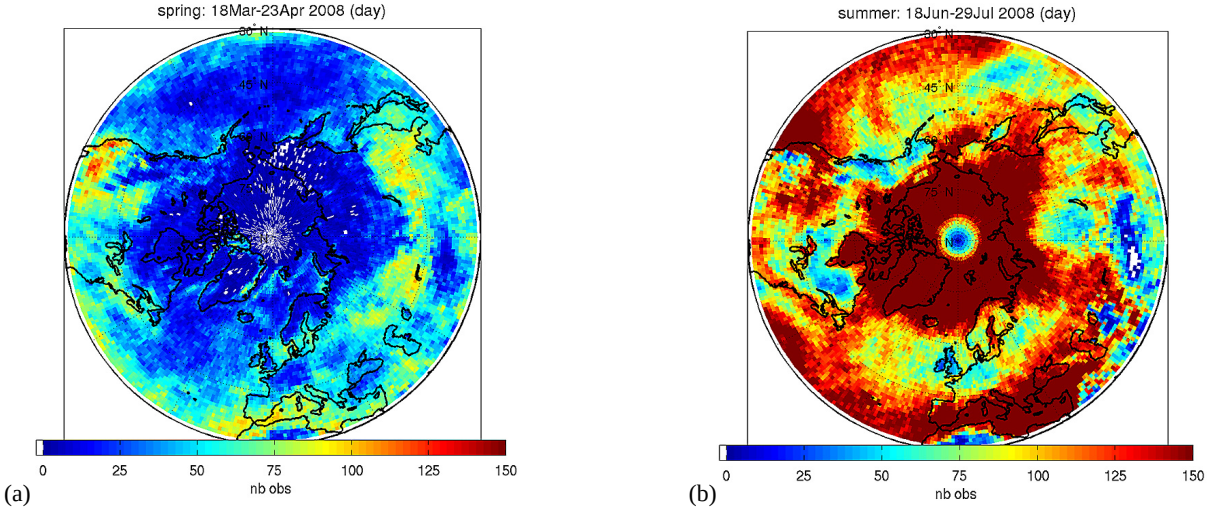

(a) (b)

Fig. 2. Distribution of the number of daytime IASI data gridded on $1° \times 1°$ using the RMS and bias filter for the spring **(a)** and summer **(b)** POLARCAT campaigns. White areas indicate no data.

level (see the lines in Fig. 3). For example, the rows characterizing IASI sensitivity between 24 and 27 km show that part of the information is coming from lower altitudes between 8 and 11 km. During both seasons that were studied in 2008, the DOFS for the total column varied between more than 1.0 (always above 65° N) to 4.0 in the Northern Hemisphere.

Figures 4 and 5 show the IASI O_3 [0–8 km] partial columns together with the corresponding DOFS distributions for spring and summer, respectively. The Arctic is characterized by higher O_3 [0–8 km] columns in spring (Fig. 4a) (mean value above 65° N $\sim 8.4 \times 10^{17}$ molec cm^{-2} during the day and the night) compared to summer (Fig. 5a) (mean value above 65° N $\sim 6.5 \times 10^{17}$ molec cm^{-2} during the day) and by low [0–8 km] DOFS values. In spring, the DOFS for the [0–8 km] column reach 0.6 during daytime and 0.8 during night-time (Fig. 4b). During the summer, DOFS reach 0.7, both in daytime and for the few pixels during night (Fig. 5b).

3 Aircraft O_3 measurements used for evaluation

3.1 In situ aircraft measurements

During POLARCAT, aircraft were deployed over the Arctic, sub-Arctic, North America, Scandinavia, Greenland and Siberia measuring a suite of trace gases, aerosols and aerosol

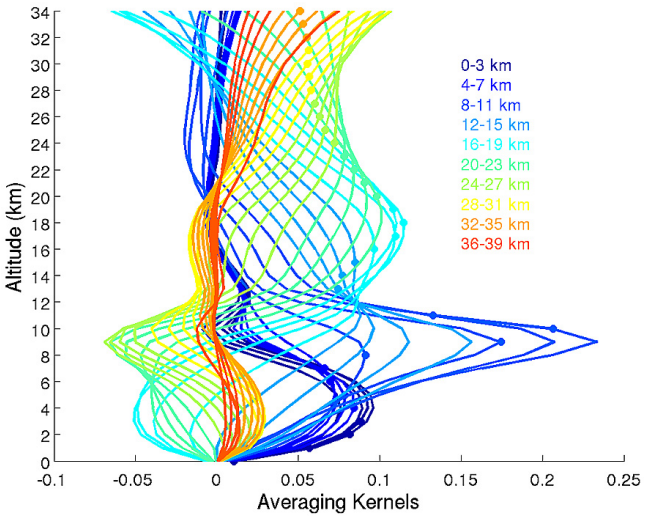

Fig. 3. Averaging kernel functions for different altitudes from FORLI-O_3 retrievals (DOFS = 3.3) at 63.7° N, 20.4° W, on 17 July 2008.

properties. Table 1 summarizes the O_3 measurements techniques used on the aircraft during the different campaigns with flight tracks as shown in Fig. 1. The French ATR-42, based in northern Sweden (spring) and Greenland (summer), and the Russian Antonov-30 aircraft over Siberia (de Villiers et al., 2010; Paris et al., 2009) both used a dual-beam UV absorption model 49–103 from Thermo Environment Instruments, USA (Thouret et al., 1998), calibrated against a NIST (National Institute of Standards and Technology) referenced O_3 calibrator Model49PS at zero, 250, 500 and 750 ppbv. Comparison with the German DLR Falcon-20 data at two altitudes revealed a 4 ppbv negative difference between the ATR-42 and the Falcon-20 related to a slight O_3 loss in the ATR-42 air inlet (e.g. 10 % for 40 ppbv and 5 % for 80 ppbv). The ATR-42 data has been corrected in this study.

The American NASA DC-8 (Ridley et al., 1992) and the NOAA WP-3D (Ryerson et al., 1998) O_3 measurements are both based on NO-induced chemiluminescence, with instrument sensitivity calibrated by standard additions of O_3 determined by UV optical absorption at 254 nm. On board the WP-3D, uncertainties in the individual O_3 measurements are typically ±0.05 ppbv (±4 % of the signal) and were verified by comparing data taken during wingtip comparison flights during the POLARCAT campaigns. Uncertainties in the DC-8 O_3 data are typically ±0.1 ppbv or ±5 % of the signal. Both aircraft flew over Alaska and the Arctic during the spring with the DC-8 flying mainly over Canadian forest fire regions in summer (Jacob et al., 2010; Brock et al., 2011).

The German DLR Falcon-20 was based in Greenland during summer 2008 and used an UV absorption instrument to measure O_3 (Schlager et al., 1997; Roiger et al., 2011). Uncertainties are typically ±2 ppbv (±5 % of the signal).

3.2 Lidar measurements

Measurements of O_3 profiles through the UTLS were made using airborne lidar from the ATR-42 aircraft during the POLARCAT-France summer campaign. The lidar was mounted to perform ozone upward looking vertical profiles in a zenith-viewing mode which limits the number of data available in the lower troposphere, below 3 km. The measurement range is of the order of 6 km above the aircraft altitude with 300 m vertical resolution and 2 min temporal resolution. The system is described in Ancellet and Ravetta (1998), while performance during various airborne applications is given in Ancellet and Ravetta (2003). Numerous comparisons have been conducted with in situ measurements (ECC ozonesonde of airborne UV photometer) showing no specific biases in clear air measurements. Measurements taken near clouds or thick aerosol layers are not included here since corrections of systematic errors related to aerosol interference are unreliable. For this study, we use profiles recorded during flight sequences at constant altitude although this limits the number of data available in the lower troposphere.

4 Methodology

4.1 ACE-FTS O_3 climatology

Airborne measurements during POLARCAT were limited to altitudes below 12 km even with the addition of the ozone lidar data. Therefore, in order to complement the aircraft profiles, we used data from the ACE-FTS (Atmospheric Chemistry Experiment-Fourier Transform Spectrometer) operational retrievals (version 2.2 ozone update; Dupuy et al., 2009) to construct an O_3 climatology for spring and summer. ACE-FTS was launched on board the Canadian SCISAT-1 satellite on 12 August 2003 into low Earth circular orbit (650 km) with high inclination (74°) (Bernath et al., 2005). It uses a high-resolution Fourier Transform Spectrometer (0.02 cm^{-1}) measuring infrared radiation from 750 to 4400 cm^{-1}in solar occultation mode to observe vertical profiles of numerous trace species and operates with an effective vertical resolution of 3–4 km (Bernath et al., 2005; Coheur et al., 2007). Daily ACE-FTS measurements are obtained for up to fifteen sunrises and fifteen sunsets and O_3 profiles are retrieved by analysing the sequence of spectra in occultation mode with a global fit algorithm (Boone et al., 2005). The altitude range of the O_3 retrievals typically extend from ∼ 10 km to ∼ 95 km (Dupuy et al., 2009). A consistent set of 37 micro-windows around 10 µm (from 985 to 1128 cm^{-1}), is used for the O_3 retrievals (Boone et al., 2005).

The O_3 climatology is constructed in the same way as described for CO in Pommier et al. (2010). All the ACE-FTS O_3 data between 2004 and 2009 are averaged seasonally. The data between February and May are used for the spring climatology and between June and September for the summer

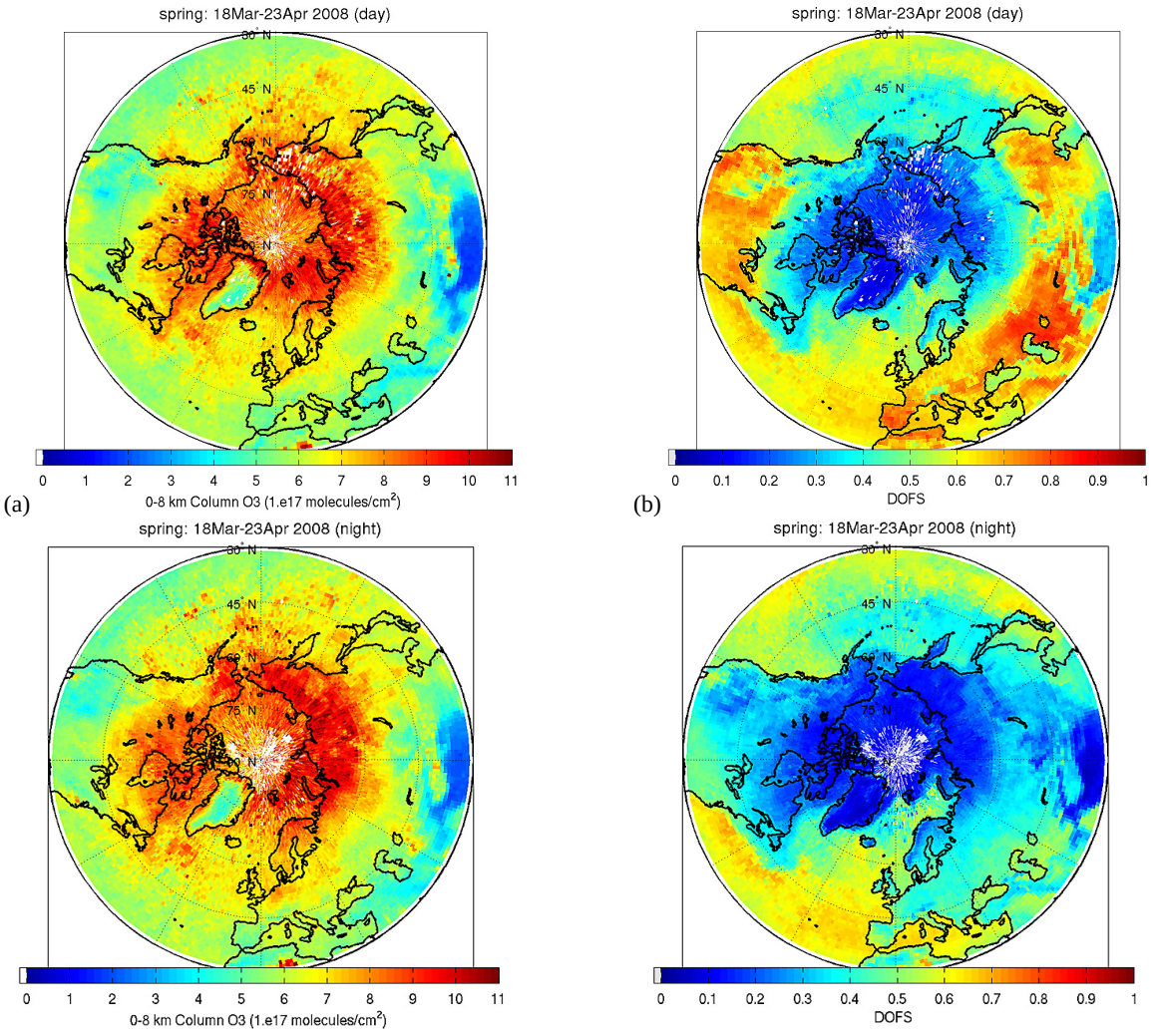

Fig. 4. Maps of IASI [0–8 km] O_3 columns **(a)** and corresponding DOFS **(b)** on a 1° × 1° grid for the spring campaign for daytime (top) and night-time (bottom). White areas indicate no data.

climatology. The data are also averaged over 15 degree latitude bins up to 60 km, where 60 km corresponds to the maximum retrieval altitude for IASI profiles, and so represents the "top of the atmosphere".

4.2 Collocation and smoothing

In this study, collocation criteria of [±0.5°, ±2 h] are used in order to locate IASI pixels close to the flight tracks. These criteria are based on a compromise between obtaining a representative number of IASI observations and ensuring that they were observed in the same meteorological conditions as the aircraft measurements.

For this validation of satellite data against airborne measurements, we follow the convention of Rodgers and Connor (2003): the FORLI-O_3 AK (**A**) and the a priori profile ($\boldsymbol{x}_a$) are applied to the aircraft profile ($\boldsymbol{x}$) in order to derive a smoothed version of the profile that would be measured by IASI. The smoothed profile is obtained as follows:

$$\boldsymbol{x}_{\text{smoothed}} = \mathbf{A}\mathbf{x} + (\mathbf{I} - \mathbf{A})\boldsymbol{x}_a \quad (1)$$

In order to fully use the averaging kernel matrix, the in situ profiles are supplemented with the ACE-FTS climatology above the maximum altitude of each aircraft. Since only a few lidar profiles are available in the lower troposphere, the lidar profiles are also completed with the FORLI a priori profile below, in addition to the ACE-FTS climatology above. This a priori will not provide more information to the smoothed profile but allows the use of the lower part of the averaging kernel matrix. An alternative technique would be to supplement the aircraft profiles with results from a chemistry transport model. However, modelling of POLARCAT data shows discrepancies compared to the data with, for example, underestimation of O_3 in the mid-troposphere (e.g. Alvarado et al., 2010).

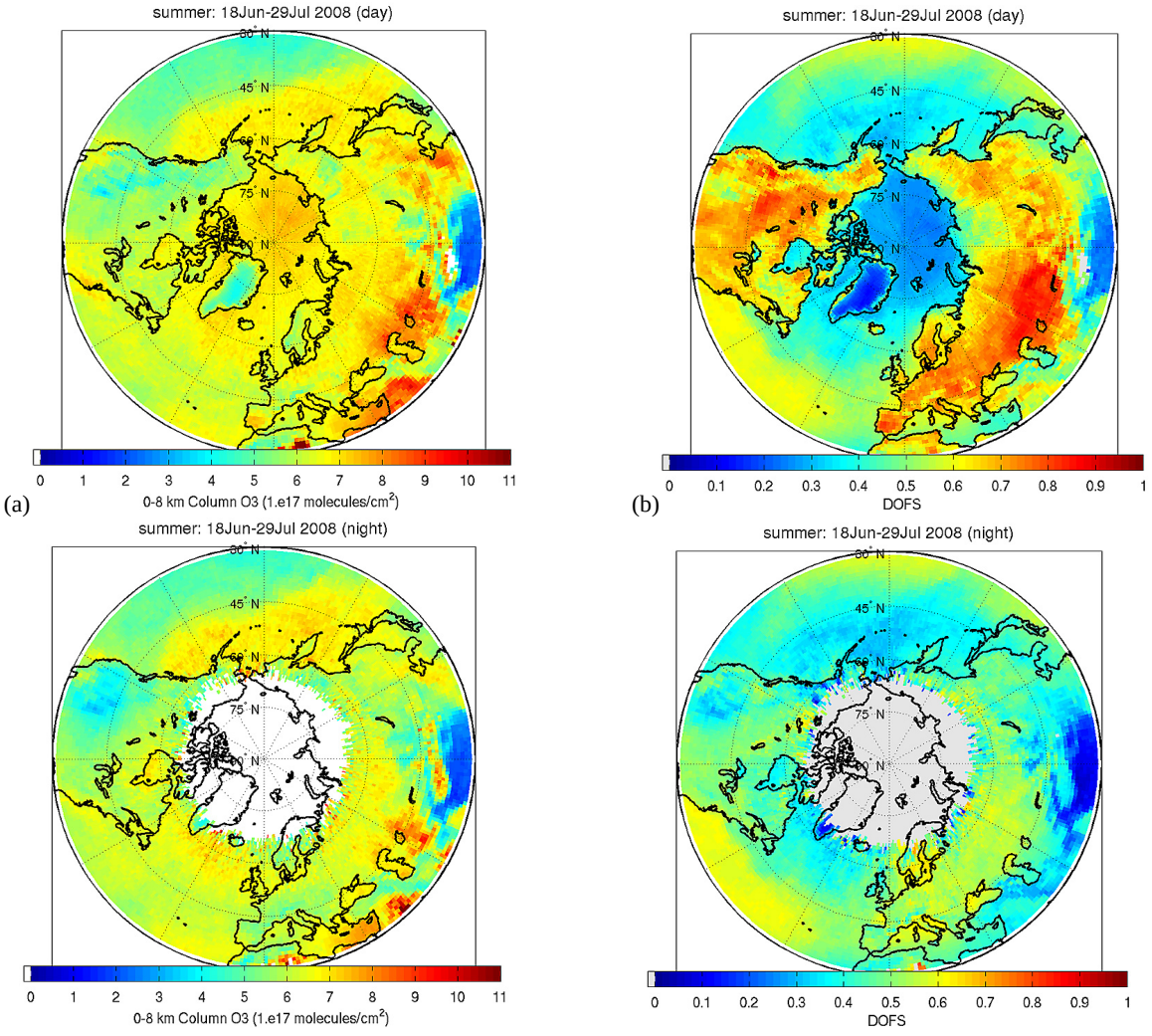

Fig. 5. Same as Fig. 4 for the summer period. White areas indicate no data.

In the following sections, we refer to in situ aircraft profiles completed using the ACE-FTS climatology (and convolved with IASI AK) as "smoothed in situ profiles". The profiles including ozone lidar measurements are called "smoothed lidar profiles".

5 Results

5.1 Aircraft average comparison

All IASI and smoothed profiles are averaged both by season and by aircraft. We compare the IASI retrievals for each aircraft because the different aircraft did not fly in the same regions, nor at the same altitudes (e.g. the ATR-42 and Falcon-20 over Greenland), nor at the same time of year as shown in Fig. 1. The aircraft also sampled different air masses ranging from flights over boreal fires, downwind of anthropogenic emissions, and stratospheric air masses. It is important to keep in mind that the retrieved profiles from IASI have coarse vertical resolution providing information over approximately 6 km altitude bins and therefore contain signatures from a mixture of air masses at different altitudes.

Figures 6 and 7 show the comparison between the mean of the FORLI retrieved O_3 profiles and the mean of the smoothed in situ profiles for each aircraft over the spring and summer campaigns, respectively. The mean tropopause height (defined hereafter using PV units equal to 2), calculated from ECMWF data, is also provided at the location of the aircraft measurements. The comparison is also performed for [0–8 km] and [0–12 km] partial columns. It is worth noting that the ACE-FTS climatology can influence results for the [0–8 km] and [0–12 km] columns. A sensitivity test increasing the climatology by 10 % leads to increases in the relative percentage difference (RD) between IASI and the data of ∼ 5 % in the case of the [0–8 km] columns and a decrease of ∼ 6–7 % for [0–12 km] columns. More IASI data

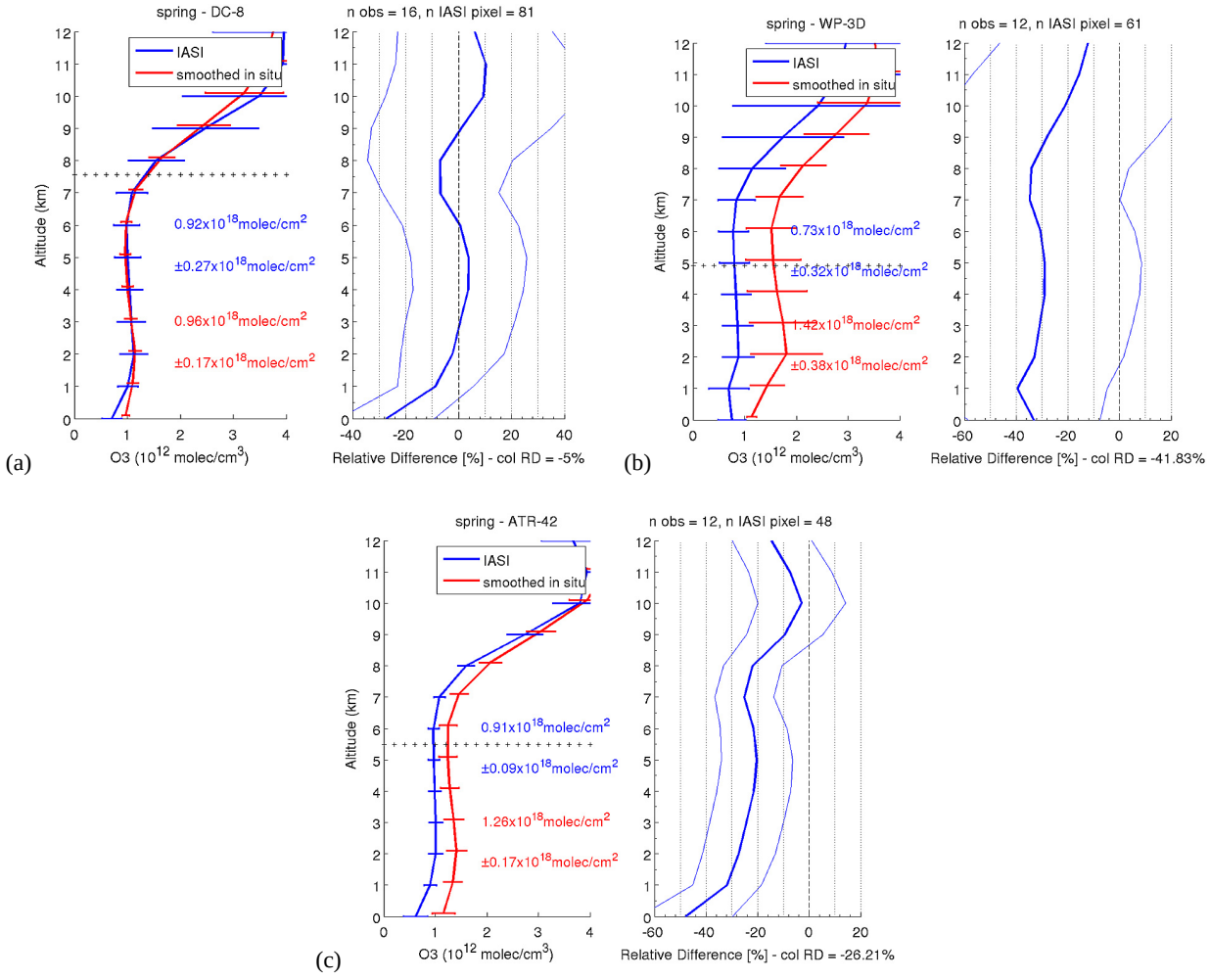

Fig. 6. Left panel: average IASI O_3 profiles (blue lines) and smoothed in situ profiles (red lines) in units of 10^{12} molecules cm^{-3} for each spring aircraft campaign; the horizontal dashed black line represents the mean position of the maximum altitude reached by each particular aircraft. Error bars represent the variability of averaged smoothed data (standard deviation $\pm 1\,\sigma$). The coloured numbers indicate the average [0–8 km] columns in 10^{17} molecules cm^{-2} together with the standard deviation. Right panel: average relative difference (RD) in % (thick blue lines for profiles and numbers below the graphs on the right are the average differences for [0–8 km] columns) and $\pm 1\,\sigma$ (thin blue lines). The number of in situ observations and IASI co-located pixels are noted at the top of the panels on the right. The relative differences are calculated as follows: [(IASI – smoothed in situ)/(smoothed in situ)] × 100 %. The smoothed in situ profiles are the in situ aircraft measurements completed with the ACE-FTS climatology and convolved with IASI AK (see text for details). Results are shown for the DC-8 **(a)**, the WP-3D **(b)** and the ATR-42 **(c)**. The mean ECMWF dynamical tropopause is at 8, 8.5 and 7.8 km, respectively.

co-located with the aircraft measurements were collected in summer (maximum of 317 pixels – Fig. 7a) compared to the spring (maximum of 81 pixels – Fig. 6a). The DC-8 provides more co-located data due to the long distances covered by the flights (Fig. 1). In spring, there are less co-located data because the satellite was often in calibration mode, as reported in Sect. 2.1.

5.1.1 Evaluation in Arctic free troposphere using in situ aircraft measurements

In general, the RDs between average IASI O_3 concentrations and the in situ part of the averaged smoothed in situ profiles (below the horizontal dashed black line – mostly below 8 km) are below 40 % at each level in spring (Fig. 6) except for the first altitude level of the ATR-42 (see Fig. 6c). This is also the case for the summer campaign (Fig. 7). These RDs are lower (below 20 %) between 2 and 7 km in most cases, showing similar results as the TES validation with ozonesondes in the Boxe et al. (2010) study. Comparison with the different aircraft show similar features with average smoothed in situ data higher than IASI O_3 in spring. This is also the case for the summer campaigns below 9 km. The average smoothed in situ [0–8 km] partial columns are always higher than those retrieved from IASI (Figs. 6 and 7). This bias is probably due to limited vertical sensitivity in IASI data at these altitudes.

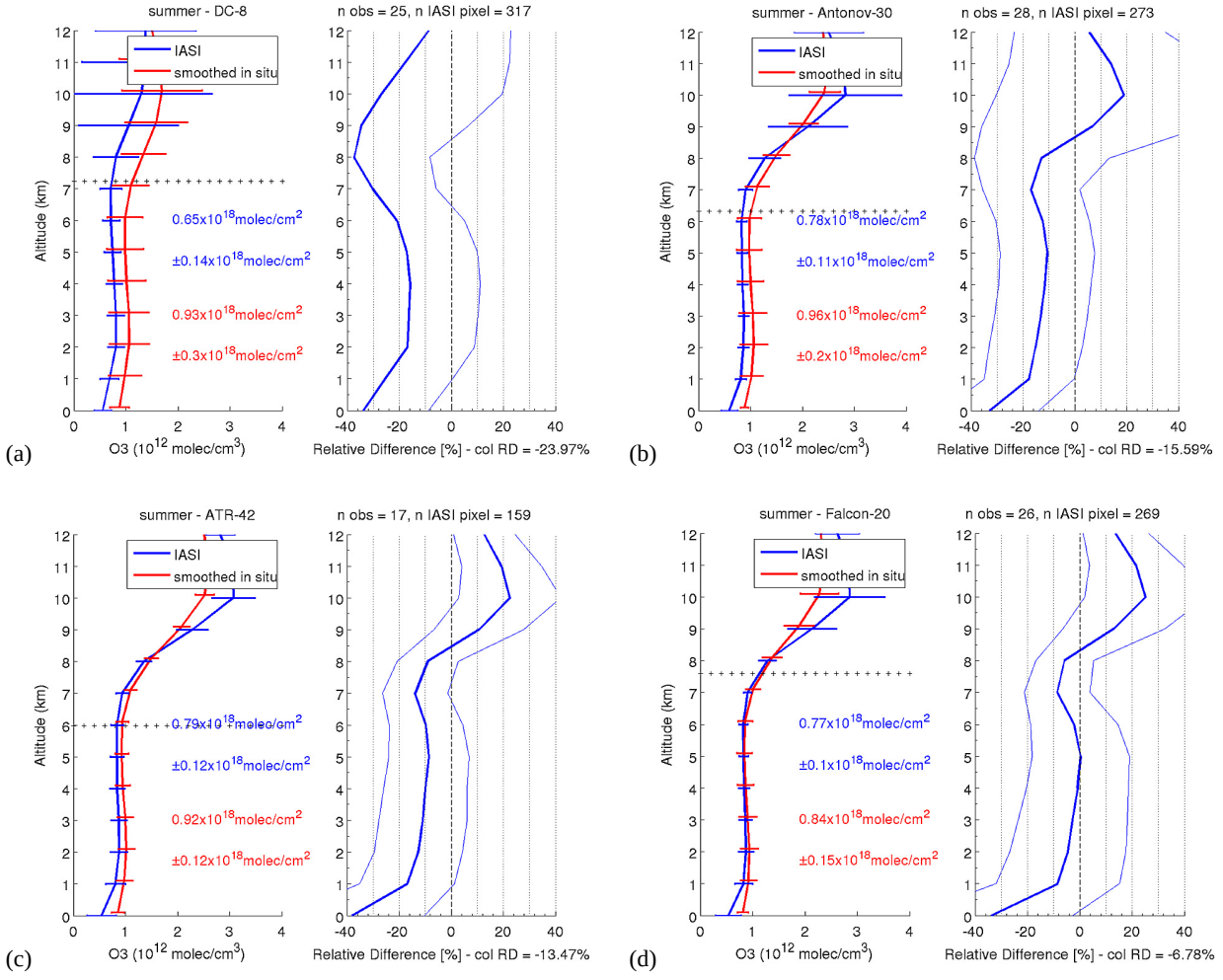

Fig. 7. Same as Fig. 6 for the aircraft involved in the summer campaigns: DC-8 **(a)**, Antonov-30 **(b)**, ATR-42 **(c)**, Falcon-20 **(d)**. The mean ECMWF dynamical tropopause is at 11.3, 9.5, 8.7 and 8.6 km, respectively.

With the exception of the DC-8 flights in spring, the correlation between IASI partial columns in the [0–8 km] range and the smoothed in situ partial columns is poor (not shown). In some cases, there is even an anti-correlation. This shows the difficulty IASI has in capturing the variability of tropospheric O_3 in the Arctic with sufficient precision as already noted in the discussion about the DOFS distribution (Figs. 4b and 5b). The poor agreement is possibly due to the low altitude of the tropopause (at around 8.1 km in spring and 9.2 km in summer) which, combined to the limited vertical sensitivity causes large overestimations of the retrievals in the UTLS as discussed further in the next section.

The correlation between IASI O_3 and the smoothed in situ O_3 from the DC-8 in spring shows better results ($r = 0.68$) whilst data from NOAA WP-3D aircraft, flying in the same region north of Alaska, are anti-correlated with IASI [0–8 km] partial columns. This difference between both American aircraft is also observed in the bias with [0–8 km] columns and in the in situ part of the average smoothed in situ profiles (0–7.6 km with the DC-8 and 0–4.9 km with the WP-3D) (Fig. 6a, b). The average IASI [0–8 km] partial columns are only 5 % lower than those derived from the DC-8 giving the best agreement between IASI and the aircraft data examined in this study. However, average IASI [0-8 km] partial columns are ∼42 % lower (Fig. 6a) than those derived from the WP-3D in spring (Fig. 6b). Since mean dynamical tropopause heights were very similar for both aircraft (8 km and 8.5 km respectively), differences in stratospheric influence do not explain these large differences between these aircraft. These differences may be due to the influence of different air masses that were sampled. The WP-3D sampled many plumes coming from the Siberia-Lake Baikal area and from agricultural burning in Kazakhstan-southern Russia as reported in Warneke et al. (2009). The DC-8 covered a much wider geographical area, as shown in Fig. 1, and sampled air masses originating from Asia, Siberia and North America (Fisher et al., 2010). The difference between these two aircraft was already noted in CO measurements (Pommier et

al., 2010), but was less pronounced. Over Scandinavia, with the ATR-42, the bias in the partial columns is around 26 %.

In summer the average IASI partial columns show a higher negative bias compared to DC-8 data (Fig. 7a) than in spring (Fig. 6a). The Russian Antonov-30 was flying over Siberia in summer sampling air masses that were occasionally influenced by boreal fires, but otherwise rather clean lower tropospheric air masses were observed (Paris et al., 2009). A strong anti-correlation with IASI is found for the [0–8 km] partial columns over Siberia. These columns are also biased by 15.6 % (Fig. 7b). Similar results are found for the ATR-42 profiles (between 1 and 6 km) and with the partial columns (RD $\sim$ 13.5 %) (Fig. 7c). The ATR-42 flew through a mixture of aged pollution plumes and clean background air masses. Among the comparison dataset, IASI O_3 agrees best with data from the Falcon-20, which also flew over Greenland, compared to ATR-42, between 1 and 7 km (Fig. 7c, d) and with the partial columns (RD $\sim$ 6.8 %).

5.1.2 Evaluation using ozone lidar measurements: free troposphere and UTLS

Figure 8 shows the comparison with upward looking ATR-42 ozone lidar measurements which provide O_3 profiles up to about 6 km above the aircraft flight altitude. The observations are separated into lidar profiles obtained for flight altitudes of less than or equal to 4 km (Fig. 8a) and for flight altitudes above 4 km (Fig. 8b). When the aircraft flew below 4 km, the lidar collected data ranging between 3.5 and 8.8 km which can also be compared to in situ O_3 measurements (mainly collected below 6 km on the ATR-42). When the aircraft was above 4 km, the lidar data ranged between 6.8 and 12.3 km and they are more representative of the UTLS over Greenland with a mean dynamical tropopause at 8.8 km. These data can be used to validate higher altitude measurements in the IASI profiles as well as the [0–12 km] partial columns.

At altitudes below 8 km, IASI shows small biases in comparison to the smoothed lidar profile (10 %) except at the surface (Fig. 8a). Note that in the part of the profile where the ACE-FTS climatology is used (above 8.8 km on average) there is a large positive bias of 64 % at 10 km. The agreement is poorer between the average retrieved IASI profiles and the average smoothed lidar O_3 profiles, using lidar data above 4 km, with differences reaching 130 % at 10 km (Fig. 8b). These differences are due to the lack of vertical resolution in the IASI retrievals and the correlation of vertical information with retrieved profile in the stratosphere (see Fig. 3). Dufour et al. (2012) already reported a bias of $\sim$ 20 % in the UTLS between IASI and ozonesondes. The upper tropospheric biases may also be due to the use of an inaccurate temperature or pressure broadening coefficient in the spectroscopy database in this region. As explained in Dufour et al. (2012), systematic errors in the linewidth from the database could imply altitude dependent biases because of compensatory effects. We also note that average IASI [0–12 km] partial columns are higher than average smoothed lidar partial columns as a result of the O_3 overestimation by IASI in the tropopause region.

IASI O_3 is also compared to in situ data from other aircraft flying in the UTLS region and shows a smaller bias of $\pm$20–30 % in summer. IASI underestimates O_3 at 9–10 km compared to the smoothed in situ concentrations derived from DC-8 data but overestimates data collected by the Falcon-20 (not shown). The differences between both aircraft could be linked to the area covered. The Falcon-20 flew over Greenland and thus sampled a range of air masses in the UTLS and the DC-8, on the other hand, covered a large geographical area during flights to the high Arctic and in North America. This is reflected in the mean dynamical tropopause heights of 8.6 km and 11.3 km, respectively (Fig. 7d, a). IASI also slightly overestimates smoothed in situ DC-8 O_3 collected in the spring (by $\sim$ 3 % at 9 km) (not shown). In summary, the Arctic UTLS O_3 concentrations retrieved by FORLI do not compare well in summer with the reference data considered here but with a mix of positive bias (high positive bias compared to the lidar and low bias with the Falcon-20) and negative bias (DC-8).

Overall, this analysis shows that the FORLI O_3 concentrations in the Arctic have the largest differences compared to the correlative aircraft measurements in the UTLS and to a lesser extent at the surface. While the latter differences probably relate to the generally weak sensitivity of IASI to the Arctic boundary layer (low thermal contrasts), the former is not yet fully explained. It could be due in part to the limited vertical resolution and/or to the use of a global covariance matrix, which causes undesired mixing between tropospheric and stratospheric concentrations, but may also be linked spectroscopic problems.

5.2 Influence of the surface properties

The comparisons are also performed according to the surface type especially since the surface type can change between spring and summer in the Arctic with many spring profiles over sea ice or snow. The land and sea criteria are chosen according to the surface altitude calculated from the global digital elevation model GTOPO30 (http://eros.usgs.gov/#/Find_Data/Products_and_Data_Available/gtopo30_info). In general, the vertical sensitivity for the total column is the same over land and sea during both seasons, characterized by a DOFS around 2.8 in spring and 3.3 in summer. This slight difference in DOFS for total columns in summer is due to higher sensitivity from 0 to 6 km over land, explained by a better thermal contrast (Clerbaux et al., 2009). This was already observed with the CO retrievals (Pommier et al., 2010). Over sea, higher vertical sensitivity between 6 and 12 km is also observed. The thermal contrast has a large impact on the sensitivity in the first layers over land, with a DOFS for the [0–8 km] range around 0.75 in summer, whilst it is lower ($\sim$ 0.4) for the spring and over sea in summer.

Table 1. Summary of O_3 in situ measurements on board the five aircraft used for this validation study and involved in POLARCAT. In addition to in situ measurements, O_3 lidar measurements are also described for the ATR-42 (last line).

Aircraft	Reference	Technique	Averaging time	Accuracy	Precision	Detection Limit	Mean of the altitude range of profiles used*
DC-8	Ridley et al. (1992)	NO-induced chemiluminescence	1 s	5%	0.1 ,ppbv	0.03 ppbv	0–7.6 km (sp) 0–7.2 km (su)
WP-3D	Ryerson et al. (1998)	NO-induced chemiluminescence	< 1 s	4 %	0.05 ppbv	0.01 ppbv for a 10-s average	0–4.9 km (sp)
Antonov-30	Paris et al. (2008), Thouret et al. (1998)	dual-beam UV absorption	4 s	2 %	2 ppbv	1 ppbv	0–6.3 km (su)
Falcon-20	Schlager et al. (1997)	UV absorption	4 s	5 %	2 ppbv	1 ppbv	0–7.6 km (su)
ATR-42	Thouret et al. (1998)	dual-beam UV absorption	4 s	2 %	2 ppbv	1 ppbv	0–5.5 km (sp) 0–6 km (su)
ATR-42	Ancellet and Ravetta (2003)	UV DIAL Lidar	2 min	7 %	5 %	na	6.5–11.9 km (su)

* sp = spring, su = summer

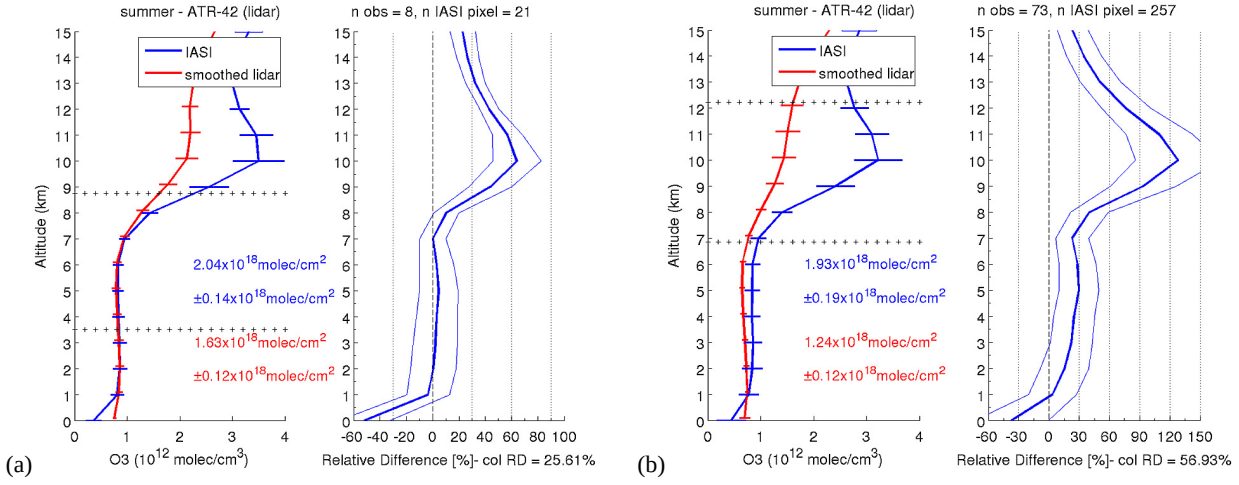

Fig. 8. Left panel: average IASI O_3 profiles (blue lines) and smoothed ATR-42 lidar profiles (red lines) in units of 10^{12} molecules cm^{-3}. Lidar profiles are separated according to the flight altitude of the ATR-42, below or equal to 4 km **(a)** and above 4 km **(b)**. The upper horizontal dashed black line represents the mean altitude where the lidar profile ends and the climatology starts. The lower horizontal dashed black line represents the mean altitude where the a priori profile ends and the lidar profile starts. Error bars represent the variability of averaged smoothed data (standard deviation $\pm 1\sigma$). The coloured numbers indicate the average [0–12 km] column in 10^{17} molecules cm^{-2} and the standard deviation. Right panel: average relative difference (RD) in % (thick blue lines for profiles and numbers below graphs on the right are the average differences for [0–12 km] columns) and $\pm 1\sigma$ (thin blue lines). The number of lidar observations and IASI co-located pixels are noted at the top right of the panels. The relative differences are calculated as follows: [(IASI – smoothed lidar)/(smoothed lidar)] × 100 %. The smoothed lidar profiles are the measurements completed with the ACE-FTS climatology and the a priori profile, and convolved with IASI AK (see text for details). The mean ECMWF dynamical tropopause is at 8.4 and 8.8 km, respectively.

Figure 9 summarizes the comparisons between IASI and in situ measurements for all aircraft during both seasons. Whatever the season and the surface type, the average smoothed in situ profiles are higher than IASI. This difference is less than 25 % over sea (Fig. 9a, c). Over land, except at the surface level where the difference reaches ∼ 40 %, RDs are less than 33 % in spring (Fig. 9b) and less than 20 % in summer (Fig. 9d). A seasonal difference is also observed for the [0–8 km] IASI columns over land which are less biased in summer (by less than 15 %) than in spring (by less than 26 %) which could be due to the difference in vertical sensitivity. Over sea, where the [0–8 km] DOFS does not vary seasonally, the RDs are similar in both seasons (≤ 14 %). Figure 10 shows a similar comparison using the ATR-42 O_3 lidar measurements. As discussed in Sect. 5.1.2, the lidar profiles are separated according to the aircraft altitude. All profiles measured below or equal to 4 km were measured over land and correspond to those already shown in Fig. 8a. For the lidar profiles collected when the aircraft was flying above 4 km, 61 profiles were collected over land and 12 profiles over sea (Fig. 10a, b). Large biases are found at 10 km in both cases with only slightly lower differences over sea

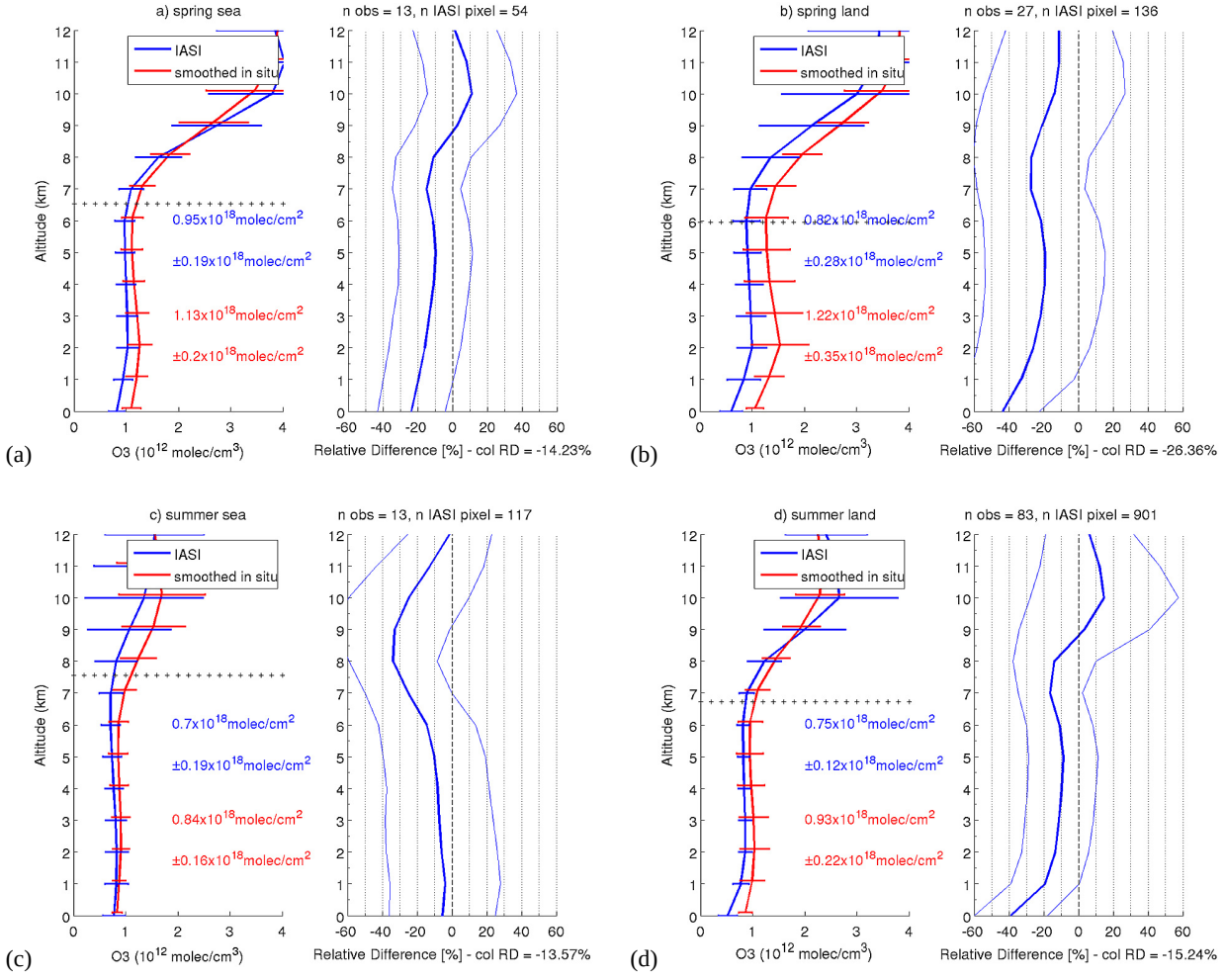

Fig. 9. Left panel: average IASI O_3 profiles (blue lines) and smoothed in situ profiles (red lines) in units of 10^{12} molecules cm^{-3} for spring (top panels) and summer (bottom panels), over sea **(a)** and **(c)** and land **(b)** and **(d)**. The horizontal dashed black line represents the mean position of the maximum altitude reached by each particular aircraft. Error bars represent the variability of averaged smoothed data (standard deviation $\pm 1\sigma$). The coloured numbers indicate the average [0–8 km] columns in 10^{17} molecules cm^{-2} and the standard deviation. Right panel: average relative differences (RD) in % (thick blue lines for profiles and numbers below the graphs on the right are the average differences for [0–8 km] columns) and $\pm 1\sigma$ (thin blue lines) are also plotted as a function of altitude. The number of in situ observations and IASI co-located pixels are noted at the top right of the panels. The mean ECMWF dynamical tropopause is at 7.8, 8.2, 10.4 and 9.5 km, respectively.

(98 % maximum, Fig. 10a) compared to over land (134 %, Fig. 10b). For the [0–12 km] partial columns the results are similar over both surfaces, again with a large positive bias (RDs > 50 %) in the IASI results. In term of absolute values, the biases calculated in the [0–8 km] columns are similar to those calculated for the [0–6 km] IASI O_3 columns in mid northern latitudes by Keim et al. (2009) and by Dufour et al. (2012), and for the [0–8 km] IASI O_3 columns in the tropics by Dufour et al. (2012). However, the high biases found here in the [0–12 km] columns are larger than those found in the [0–11 km] columns in the studies by Keim et al. (2009) and Dufour et al. (2012).

Table 2 provides the correlation coefficients between IASI O_3 and the smoothed in situ O_3 [0–8 km] columns together with the relative differences corresponding to the spring and the summer campaigns according to surface type. Table 3 provides the correlations between IASI O_3 and the smoothed lidar O_3 [0–12 km] columns and the relative differences in summer. As noted previously, the correlation with in situ smoothed partial columns is poor with anti-correlations over land in spring and over sea in summer (Table 2). Over land, correlation with the smoothed lidar partial columns is good (0.67) below 4 km but, above 4 km, this decreases to 0.17. Results are better for the few data collected over sea (0.46). These results suggest that the FORLI retrieval has more difficulty in the UTLS over land than over sea witch probably could not be only explained by the slight difference of tropopause heights over land (8.8 km – Fig. 10b) compared

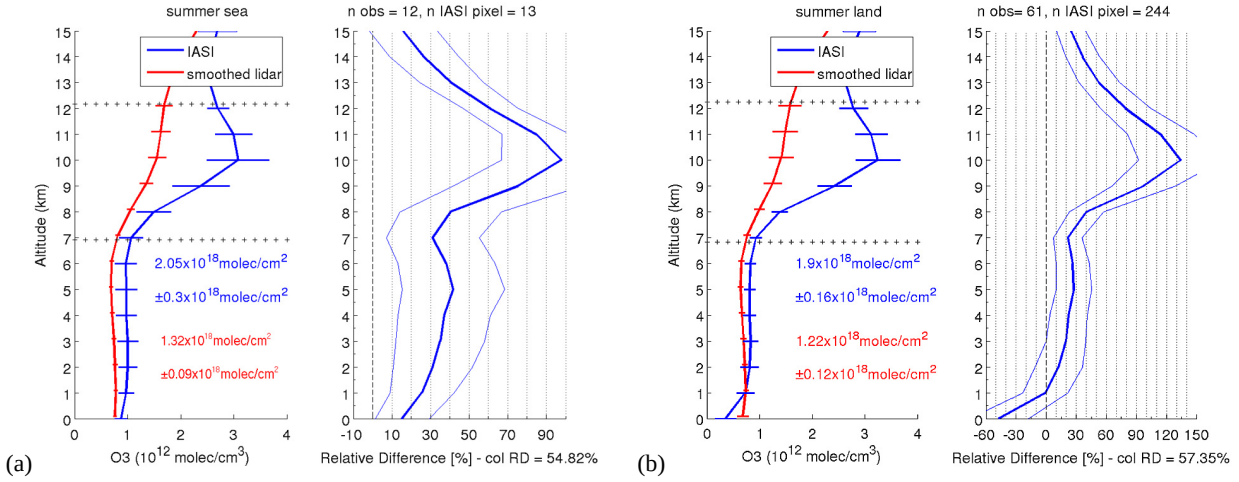

Fig. 10. Left panel: average IASI O_3 profiles (blue lines) and smoothed lidar profiles (red lines) in units of 10^{12} molecules cm^{-3} over sea **(a)** land **(b)**. Lidar profiles were measured above 4 km. The upper horizontal dashed black line represents the mean altitude where the lidar profile ends and the climatology starts. The lower horizontal dashed black line represents the mean altitude where the a priori profile ends and the lidar profile starts. Error bars represent the variability of averaged smoothed data (standard deviation $\pm 1\sigma$). The coloured numbers indicate the average [0–12 km] columns in 10^{17} molecules cm^{-2} and the standard deviation. Right panel: average relative difference (RD) in % (thick blue lines for profiles and numbers below the graphs on the right are the average differences for [0–12 km] columns) and $\pm 1\sigma$ (thin blue lines). The number of lidar observations and IASI co-located pixels are noted at the top right of the panels. The mean ECMWF dynamical tropopause is at 9.1 and 8.8 km, respectively.

Table 2. Summary of correlations between retrieved IASI O_3 and smoothed in situ O_3 [0–8 km] columns for the spring and the summer campaigns according to surface type. The number of observations is provided next to the surface type. The relative difference is given in parentheses.

	spring		summer	
	Sea – 13	Land – 27	Sea –13	Land – 83
0–8 km	0.15 (−14.2 %)	−0.33 (−26.4 %)	−0.03 (−13.6 %)	0.02 (−15.2 %)

Table 3. Summary of correlations between retrieved IASI O_3 and smoothed lidar O_3 [0–12 km] columns for the summer campaign according to surface type. The profiles are separated according to the flight altitude of the ATR-42 (threshold at 4 km). The number of observations is provided next to the surface type. The relative difference is given in parentheses.

	Sea – 12 (> 4 km)	Land – 61 (> 4 km)	Land – 8 (≤ 4 km)
0–12 km	0.46 (54.8 %)	0.17 (57.4 %)	0.67 (25.6 %)

to over sea (9.1 km – Fig. 10a). It could be due to differences in topography. As shown in Fig. 3, the first layers of the AK also have an impact on the sensitivity around 8–10 km. These differences in topography could affect the information borrowed by the AKs at these altitudes which could be too important compared to the lower troposphere ([0–12 km] DOFS ~ 1.0 over land and ~ 0.85 over sea).

5.3 IASI distributions in Arctic UTLS

The results discussed in the previous sections highlighted large differences above 9–10 km between smoothed lidar values and IASI observations. In this section, we show particular examples where IASI is able to detect variability in the tropopause region including tropospheric fold events when the tropopause is at lower altitudes. Two examples are shown in Figs. 11 and 12. The first case compares IASI data with data collected on 10 July 2008 by the Falcon-20 during a flight over central-northern Greenland. Analysis of data from this flight is discussed in detail by Roiger et al. (2011) showing that Asian polluted air had been transported into the lower stratosphere and was observed embedded within UTLS air. Sodemann et al. (2011) also discussed the transport of Asian pollution across the North Pole and compared global model simulations with IASI CO data. During this flight the tropopause altitude was in the range 8 to 10 km. This is shown by the IASI O_3 gradient (Fig. 11a) and predicted by the FLEXPART model used in the study by Roiger et al. (2011). The FORLI-O_3 retrieved concentrations, using

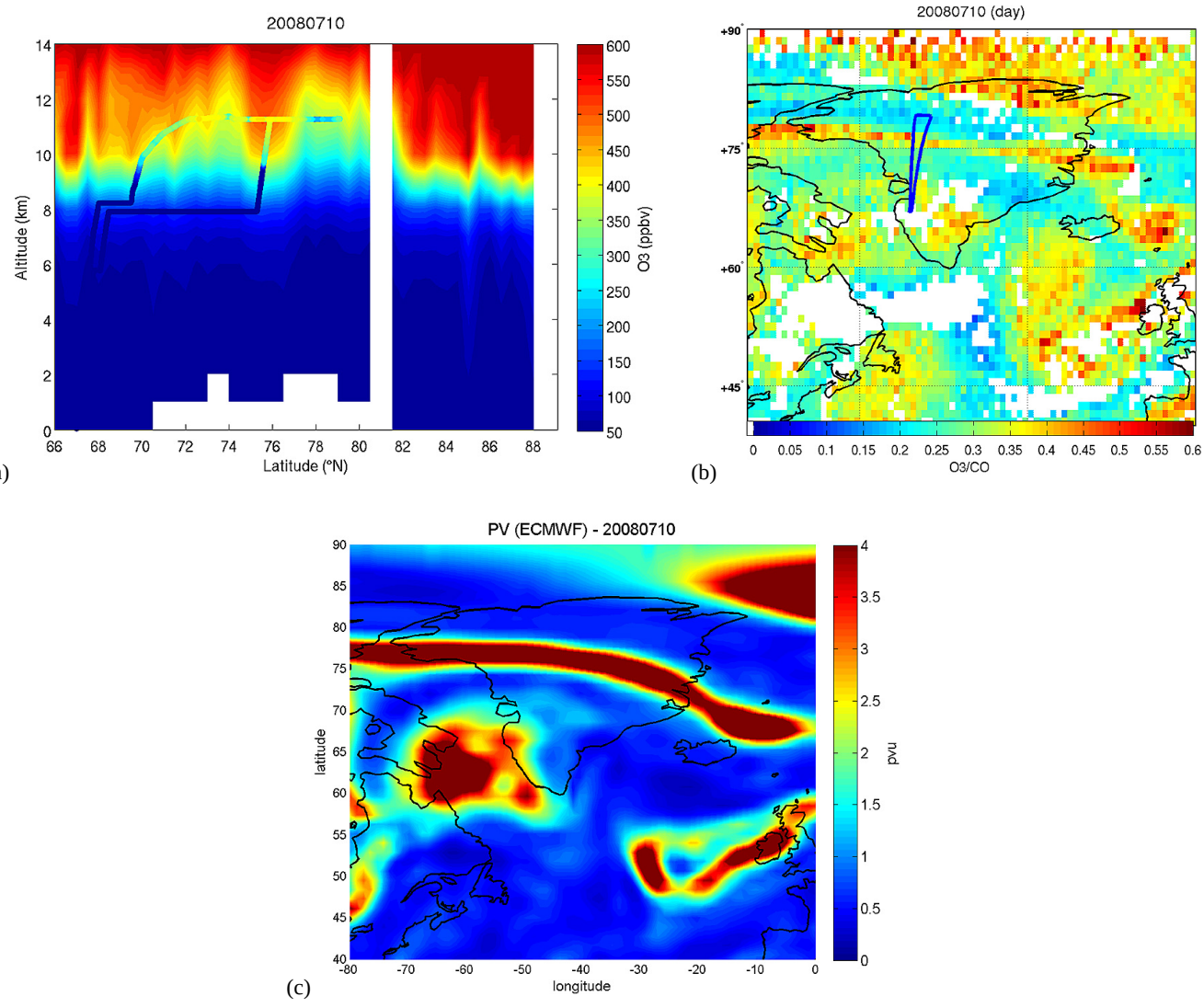

Fig. 11. (a) In situ O_3 volume mixing ratios (ppbv) measured by the Falcon-20 on 10 July 2008 compared to IASI O_3 vertical distributions along the flight. IASI data are averages data between 49° W and 51° W and sampled every 0.5° between 66° N and 89° N; **(b)** distributions of the ratio between daytime IASI O_3 [0–8 km] partial columns and IASI CO total columns over Greenland on a $1° \times 1°$ grid on 10 July 2008. The Falcon-20 flight track is plotted in blue. In **(a)** and **(b)**, white areas indicate no data; **(c)** potential vorticity (in PVU) at 8 km over Greenland taken from an ECMWF analysis data at 12:00 UTC on 10 July 2008.

temperatures measured by IASI, exhibit the same variability in tropopause altitude, as the FLEXPART model using the ECMWF data. However, the IASI O_3 concentrations retrieved by FORLI in the UTLS (> 300 ppbv) are too high, as also discussed in Sect. 5.1.2. Figure 11b shows the ratio between IASI O_3 [0–8 km] columns and IASI CO total columns (only ~ 17 % of the CO is above 8 km, Pommier et al., 2010). Variability in this ratio provides information about air masses influenced by the stratosphere between the surface and 8 km when O_3 [0–8 km] columns are higher. Since only 17 % of CO total columns reside in the stratosphere this quantity is primarily sensitive to tropospheric sources. The calculated O_3 / CO ratio is relatively well correlated with the potential vorticity (PV) map from ECMWF analysis data (Fig. 11c), where the dynamical tropopause is equal to 2 PVU. In the northern part of the flight ($> 75°$ N), the Falcon-20 first crossed a stratospheric air mass (high O_3 / CO filament in Fig. 11b and high PV in Fig. 11c), and then the polluted plume from Asia (low O_3 / CO ratios).

Figure 12 shows results for a flight of the ATR-42 on 7 July 2008 when the ozone lidar also made measurements. This flight was made over southern Greenland during a period when air masses were advected from North America (Schmale et al., 2011; Quennehen et al., 2011). In situ O_3 data together with retrieved IASI O_3 profiles are shown in Fig. 12a and ozone lidar data along the flight in Fig. 12b.

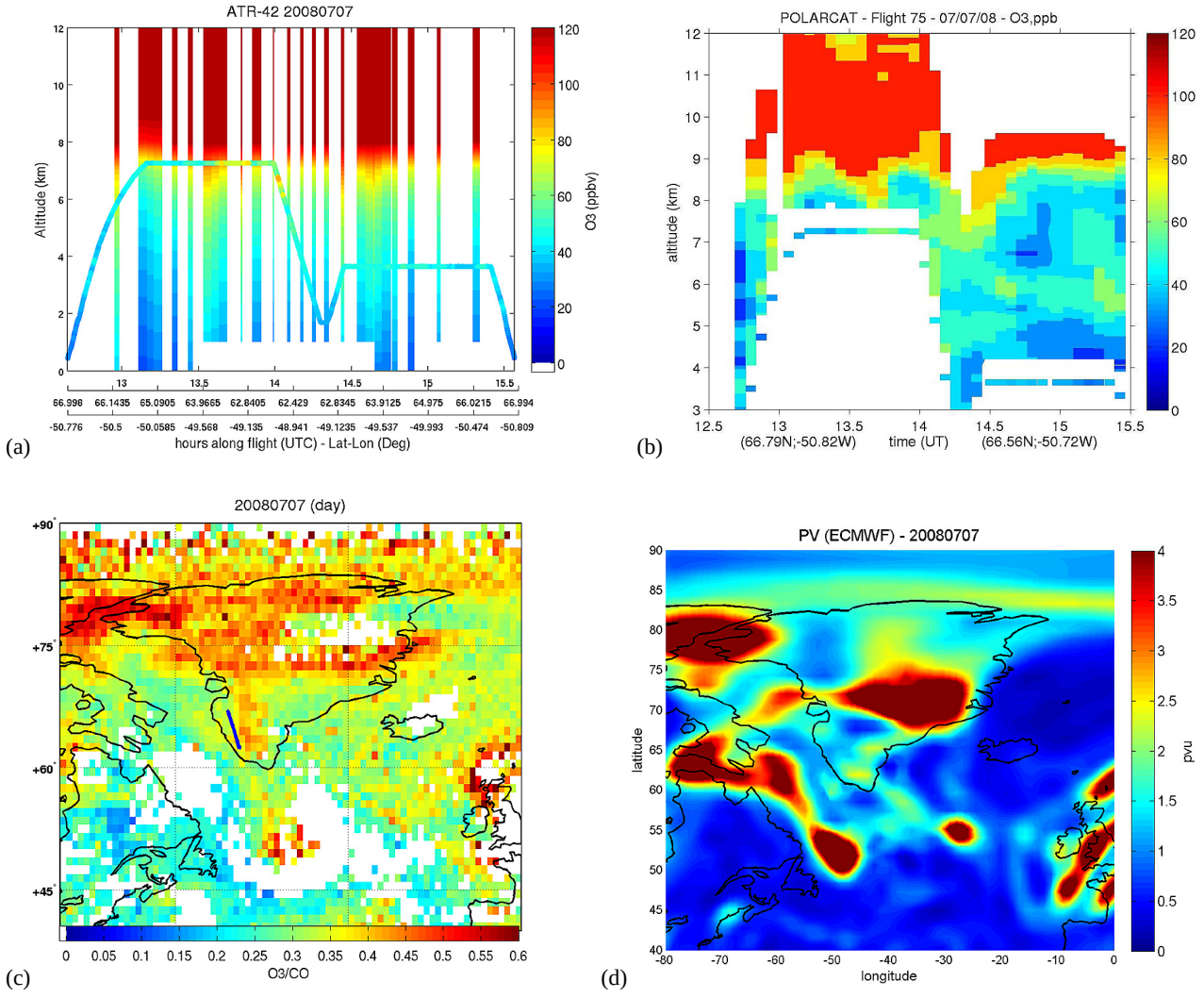

Fig. 12. In situ O_3 volume mixing ratios (ppbv) measured by the ATR-42 on 7 July 2008 compared to co-located IASI O_3 vertical distributions (using a criteria of [$\pm 0.2°$; ± 1 h]) along the flight **(a)** and O_3 lidar vertical measurements **(b)**. In situ **(a)** and lidar **(b)** data are plotted as a function of altitude versus time (UTC) along the flight track. The latitude and longitude on x-axis corresponds to the aircraft position **(a)**. Distribution of the ratio between daytime IASI O_3 [0–8 km] partial columns and IASI CO total columns over Greenland on a $1° \times 1°$ grid for 7 July 2008 with the ATR-42 flight track shown as a blue line **(c)**. White areas indicate no data. Potential vorticity (in PVU) at 8 km over Greenland from ECMWF analysis data at 12:00 UTC on 7 July 2008 **(d)**.

The vertical O_3 gradient is reasonably well captured by IASI compared to the lidar although IASI detected the steepest gradient around 7.5 km compared to 9 km in the lidar data, for example, around 13:30 UTC (10:30 LT). At the same time, the aircraft sampled a plume originating from Canadian boreal fires which was also mixed with air from the upper troposphere associated with a tropospheric fold which is visible in the ozone lidar data. This feature was detected by IASI and also later during the return leg of the flight from southern Greenland back to Kangerlussuaq at around 14:30 UTC. Due to the timing of overpasses nearest to the flight track, IASI data shows features appearing earlier than were observed by the lidar. The aircraft also flew close to another stratospherically influenced air mass during the most southerly part of the flight. This is shown as a clear feature in the IASI O_3 / CO ratio (Fig. 12c) and can also be seen to a lesser extent in the PV map (Fig. 12d) for this flight. The combined use of two IASI observations (CO and O_3), shows how IASI data can provide a useful diagnostic for the evaluation of STE episodes.

6 Conclusions

This paper compares tropospheric O_3 concentrations retrieved from the IASI satellite-borne instrument using the FORLI-O_3 algorithm with aircraft measurements obtained as part of POLARCAT in spring and summer 2008. Aircraft

data were collected in different parts of the Arctic, for air masses influenced by anthropogenic emissions, boreal forest fires over Siberia and Canada as well as air masses in the upper troposphere and the stratosphere. For comparison purposes, IASI data are selected using a collocation criterion of [±0.5°; ±2 h] with the aircraft observations. Aircraft profiles are completed with a seasonal and latitudinal climatology based on ACE-FTS data averaged from 2004 to 2009, and then convolved with IASI averaging kernels. The comparison is performed for the different aircraft campaigns which sampled different atmospheric regions, as well as against the combined measurements for the spring and summer campaigns as a function of surface type (sea and land).

On average, the vertical sensitivity in the retrieval of the IASI total columns is similar over land and sea surfaces in spring and summer, and is only slightly higher in summer (DOFS ∼ 3.3) compared to spring (DOFS ∼ 2.8). The DOFS for the column between the surface and 8 km range from 0.4 in spring to 0.75 over land in summer. IASI O_3 profiles are usually biased low between 0 and 8 km (by less than 40 % and less than 25 % over sea whatever the season), with IASI underestimating the smoothed in situ profiles in both seasons. Often the bias is reduced below 20 % between 2 and 7 km. Comparison with the ozone lidar data on the ATR-42 (complemented with the FORLI a priori profile) over Greenland shows good agreement in the free troposphere (RDs ∼ 10 %) but also reveals a high positive bias in the UTLS (above 9–10 km). These important differences in the UTLS impact the comparison with the IASI [0–12 km] partial columns and the correlations analysis. With some noticeable exceptions (such as over the land in Greenland with profiles taken below 4 km by the lidar instrument and over North America with in situ measurements, $r \sim 0.7$), the correlation coefficient between retrieved IASI O_3 partial columns and those derived from in situ or ozone lidar measurements on board the aircraft is very low. However, the [0–8 km] partial columns show low biases (by less than 15 %) over sea during both seasons and land during summer. Larger differences are found over the land in spring (∼ 26 %). In all cases, the IASI [0–8 km] partial columns are lower than smoothed in situ partial columns while the [0–12 km] partial columns are higher than the lidar smoothed partial columns. The biases in the Arctic boundary layer is related to a low thermal contrast whilst the inconsistencies in the UTLS, require further investigation. These are probably due to limited vertical resolution or to the use of a global covariance matrix, which causes undesired mixing between tropospheric and stratospheric concentrations, but may also be linked spectroscopic problems.

In spite of these differences, we show that IASI has the capacity to detect variability in O_3 concentrations and its gradient in the tropopause region including variability driven by dynamical features such as tropospheric folds. The calculated ratio between IASI O_3 [0–8 km] columns and simultaneously retrieved IASI CO total columns is a good indicator of regions influenced by stratospheric air masses. This shows that the combined use of different IASI observations could provide a useful diagnostic to supplement model forecasts as well as for evaluation of global chemical model simulations.

Acknowledgements. M. Pommier was supported by a fellowship grant from Centre National d'Etudes Spatiales (CNES, France), from NOVELTIS and from Natural Sciences and Engineering Research Council of Canada (NSERC, Canada). We thank Chris McLinden for his help and his comments on the manuscript. IASI was developed and built under the responsibility of CNES and flies onboard the MetOp satellite as part of the Eumetsat Polar system. The authors acknowledge the Ether French atmospheric database (http://ether.ipsl.jussieu.fr) for distributing the IASI L1C data. POLARCAT-France was funded by French ANR, CNES, CNRS-INSU (LEFE-CHAT), IPEV and EUFAR. We also thank INSU-LEFE CLIMSLIP for support. POLARCAT-GRACE was funded by DLR. The YAK-AEROSIB campaigns were funded by the CNRS-DRI (France), the French Ministry of Foreign Affairs, CEA (France), POLARCAT France/Norway, RAS (Russia) and RFBR (Russia), and operated in collaboration with IAO-SB-RAS, Tomsk, Russia. The ACE mission is supported primarily by the Canadian Space Agency with some funding was provided by the UK Natural Environment Research Council (NERC). The French team is grateful to CNES for continuous scientific and financial support. P.-F. Coheur is research associate with the FRS-FNRS; the research in Belgium was funded by the "Actions de Recherche Concertées" (Communauté Française), the Fonds National de la Recherche Scientifique, the Belgian State Federal Office for Scientific, Technical and Cultural Affairs and the European Space Agency (ESA-Prodex C90-327). The authors are grateful to CNRS-INSU for publication support.

Edited by: P. Monks

The publication of this article is financed by CNRS-INSU.

References

Alvarado, M. J., Logan, J. A., Mao, J., Apel, E., Riemer, D., Blake, D., Cohen, R. C., Min, K.-E., Perring, A. E., Browne, E. C., Wooldridge, P. J., Diskin, G. S., Sachse, G. W., Fuelberg, H., Sessions, W. R., Harrigan, D. L., Huey, G., Liao, J., Case-Hanks, A., Jimenez, J. L., Cubison, M. J., Vay, S. A., Weinheimer, A. J., Knapp, D. J., Montzka, D. D., Flocke, F. M., Pollack, I. B., Wennberg, P. O., Kurten, A., Crounse, J., Clair, J. M. St., Wisthaler, A., Mikoviny, T., Yantosca, R. M., Carouge, C. C., and Le Sager, P.: Nitrogen oxides and PAN in plumes from boreal fires during ARCTAS-B and their impact on ozone: an integrated analysis of aircraft and satellite observations, Atmos. Chem. Phys., 10, 9739–9760, doi:10.5194/acp-10-9739-2010, 2010.

Ancellet, G. and Ravetta, F.: Compact Airborne Lidar for Tropospheric Ozone: Description and Field Measurements, Appl. Optics, 37, 5509–5521, 1998.

Ancellet, G. and Ravetta, F.: On the usefulness of an airborne lidar for O_3 layer analysis in the free troposphere and the planetary boundary layer, J. Environ. Monitor., 5, 47–56, 2003.

Antón, M., Loyola, D., Clerbaux, C., López, M., Vilaplana, J. M., Bañón, M., Hadji-Lazaro, J., Valks, P., Hao, N., Zimmer, W., Coheur, P.-F., Hurtmans, D., and Alados-Arboledas, L.: Validation of the Metop-A total ozone data from GOME-2 and IASI using reference ground-based measurements at the Iberian Peninsula, Remote Sens. Environ., 115, 1380–1386, 2011.

Bernath, P. F., McElroy, C. T., Abrams, M. C., Boone, C. D., Butler, M., Camy-Peyret, C., Carleer, M., Clerbaux, C., Coheur, P.-F., Colin, R., DeCola, P., DeMazière, M., Drummond, J. R., Dufour, D., Evans, W. F. J., Fast, H., Fussen, D., Gilbert, K., Jennings, D. E., Llewellyn, E. J., Lowe, R. P., Mahieu, E., McConnell, J. C., McHugh, M., McLeod, S. D., Michaud, R., Midwinter, C., Nassar, R., Nichitiu, F., Nowlan, C., Rinsland, C. P., Rochon, Y. J., Rowlands, N., Semeniuk, K., Simon, P., Skelton, R., Sloan, J. J., Soucy, M.-A., Strong, K., Tremblay, P., Turnbull, D., Walker, K. A., Walkty, I., Wardle, D. A., Wehrle, V., Zander, R., and Zou, J.: Atmospheric Chemistry Experiment (ACE): Mission overview, Geophys. Res. Lett., 32, L15S01, doi:10.1029/2005GL022386, 2005.

Boone, C. D., Nassar, R., Walker, K. A., Rochon, Y., McLeod, S. D., Rinsland, C. P., and Bernath, P. F.: Retrievals for the atmospheric chemistry experiment Fourier-transform spectrometer, Appl. Optics, 44, 7218–7231, 2005.

Boxe, C. S., Worden, J. R., Bowman, K. W., Kulawik, S. S., Neu, J. L., Ford, W. C., Osterman, G. B., Herman, R. L., Eldering, A., Tarasick, D. W., Thompson, A. M., Doughty, D. C., Hoffmann, M. R., and Oltmans, S. J.: Validation of northern latitude Tropospheric Emission Spectrometer stare ozone profiles with ARC-IONS sondes during ARCTAS: sensitivity, bias and error analysis, Atmos. Chem. Phys., 10, 9901–9914, doi:10.5194/acp-10-9901-2010, 2010.

Boynard, A., Clerbaux, C., Coheur, P.-F., Hurtmans, D., Turquety, S., George, M., Hadji-Lazaro, J., Keim, C., and Meyer-Arnek, J.: Measurements of total and tropospheric ozone from IASI: comparison with correlative satellite, ground-based and ozonesonde observations, Atmos. Chem. Phys., 9, 6255–6271, doi:10.5194/acp-9-6255-2009, 2009.

Brock, C. A., Cozic, J., Bahreini, R., Froyd, K. D., Middlebrook, A. M., McComiskey, A., Brioude, J., Cooper, O. R., Stohl, A., Aikin, K. C., de Gouw, J. A., Fahey, D. W., Ferrare, R. A., Gao, R.-S., Gore, W., Holloway, J. S., Hübler, G., Jefferson, A., Lack, D. A., Lance, S., Moore, R. H., Murphy, D. M., Nenes, A., Novelli, P. C., Nowak, J. B., Ogren, J. A., Peischl, J., Pierce, R. B., Pilewskie, P., Quinn, P. K., Ryerson, T. B., Schmidt, K. S., Schwarz, J. P., Sodemann, H., Spackman, J. R., Stark, H., Thomson, D. S., Thornberry, T., Veres, P., Watts, L. A., Warneke, C., and Wollny, A. G.: Characteristics, sources, and transport of aerosols measured in spring 2008 during the aerosol, radiation, and cloud processes affecting Arctic Climate (ARCPAC) Project, Atmos. Chem. Phys., 11, 2423–2453, doi:10.5194/acp-11-2423-2011, 2011.

Clerbaux, C., Boynard, A., Clarisse, L., George, M., Hadji-Lazaro, J., Herbin, H., Hurtmans, D., Pommier, M., Razavi, A., Turquety, S., Wespes, C., and Coheur, P.-F.: Monitoring of atmospheric composition using the thermal infrared IASI/MetOp sounder, Atmos. Chem. Phys., 9, 6041–6054, doi:10.5194/acp-9-6041-2009, 2009.

Coheur, P.-F., Herbin, H., Clerbaux, C., Hurtmans, D., Wespes, C., Carleer, M., Turquety, S., Rinsland, C. P., Remedios, J., Hauglustaine, D., Boone, C. D., and Bernath, P. F.: ACE-FTS observation of a young biomass burning plume: first reported measurements of C2H4, C3H6O, H2CO and PAN by infrared occultation from space, Atmos. Chem. Phys., 7, 5437–5446, doi:10.5194/acp-7-5437-2007, 2007.

de Villiers, R. A., Ancellet, G., Pelon, J., Quennehen, B., Schwarzenboeck, A., Gayet, J. F., and Law, K. S.: Airborne measurements of aerosol optical properties related to early spring transport of mid-latitude sources into the Arctic, Atmos. Chem. Phys., 10, 5011–5030, doi:10.5194/acp-10-5011-2010, 2010.

Dibb, J. E., Talbot, R. W., Scheuer, E., Seid, G., DeBell, L., Lefer, B., and Ridley, B.: Stratospheric influence on the northern North American free troposphere during TOPSE: 7Be as a stratospheric tracer, J. Geophys. Res., 108, 8363, doi:10.1029/2001JD001347, 2003.

Dufour, G., Eremenko, M., Griesfeller, A., Barret, B., LeFlochmoën, E., Clerbaux, C., Hadji-Lazaro, J., Coheur, P.-F., and Hurtmans, D.: Validation of three different scientific ozone products retrieved from IASI spectra using ozonesondes, Atmos. Meas. Tech., 5, 611–630, doi:10.5194/amt-5-611-2012, 2012.

Dupuy, E., Walker, K. A., Kar, J., Boone, C. D., McElroy, C. T., Bernath, P. F., Drummond, J. R., Skelton, R., McLeod, S. D., Hughes, R. C., Nowlan, C. R., Dufour, D. G., Zou, J., Nichitiu, F., Strong, K., Baron, P., Bevilacqua, R. M., Blumenstock, T., Bodeker, G. E., Borsdorff, T., Bourassa, A. E., Bovensmann, H., Boyd, I. S., Bracher, A., Brogniez, C., Burrows, J. P., Catoire, V., Ceccherini, S., Chabrillat, S., Christensen, T., Coffey, M. T., Cortesi, U., Davies, J., De Clercq, C., Degenstein, D. A., De Mazière, M., Demoulin, P., Dodion, J., Firanski, B., Fischer, H., Forbes, G., Froidevaux, L., Fussen, D., Gerard, P., Godin-Beekmann, S., Goutail, F., Granville, J., Griffith, D., Haley, C. S., Hannigan, J. W., Höpfner, M., Jin, J. J., Jones, A., Jones, N. B., Jucks, K., Kagawa, A., Kasai, Y., Kerzenmacher, T. E., Kleinböhl, A., Klekociuk, A. R., Kramer, I., Küllmann, H., Kuttippurath, J., Kyrölä, E., Lambert, J.-C., Livesey, N. J., Llewellyn, E. J., Lloyd, N. D., Mahieu, E., Manney, G. L., Marshall, B. T., McConnell, J. C., McCormick, M. P., McDermid, I. S., McHugh, M., McLinden, C. A., Mellqvist, J., Mizutani, K., Murayama, Y., Murtagh, D. P., Oelhaf, H., Parrish, A., Petelina, S. V., Piccolo, C., Pommereau, J.-P., Randall, C. E., Robert, C., Roth, C., Schneider, M., Senten, C., Steck, T., Strandberg, A., Strawbridge, K. B., Sussmann, R., Swart, D. P. J., Tarasick, D. W., Taylor, J. R., Tétard, C., Thomason, L. W., Thompson, A. M., Tully, M. B., Urban, J., Vanhellemont, F., Vigouroux, C., von Clarmann, T., von der Gathen, P., von Savigny, C., Waters, J. W., Witte, J. C., Wolff, M., and Zawodny, J. M.: Validation of ozone measurements from the Atmospheric Chemistry Experiment (ACE), Atmos. Chem. Phys., 9, 287–343, doi:10.5194/acp-9-287-2009, 2009.

Engvall Stjernberg, A.-C., Skorokhod, A., Paris, J.-D., Elansky, N., Nédélec, P., and Stohl, A.: Low surface ozone in Siberia, Tellus B, 64, 11607, 2012.

Fisher, J. A., Jacob, D. J., Purdy, M. T., Kopacz, M., Le Sager, P., Carouge, C., Holmes, C. D., Yantosca, R. M., Batchelor, R. L., Strong, K., Diskin, G. S., Fuelberg, H. E., Holloway, J. S., Hyer, E. J., McMillan, W. W., Warner, J., Streets, D. G., Zhang, Q., Wang, Y., and Wu, S.: Source attribution and interannual variability of Arctic pollution in spring constrained by aircraft (ARCTAS, ARCPAC) and satellite (AIRS) observations of carbon monoxide, Atmos. Chem. Phys., 10, 977–996, doi:10.5194/acp-10-977-2010, 2010.

Garrett, T. J. and Verzella, L. L.: LOOKING BACK: An Evolving History of Arctic Aerosols, B. Am. Meteorol. Soc., 89, 299–302, doi:10.1175/BAMS-89-3-299, 2008.

Greenaway, K. R.: Experiences with Arctic flying weather, Royal Meteorological Society Canadian Branch, Toronto, Ontario, Canada, 1950.

HTAP, Hemispheric Transport of Air Pollution 2010 New York and Geneva: Air pollution studies 17, Economic commission for Europe, 2010.

Hurtmans, D., Coheur, P.-F., Wespes, C., Clarisse, L., Scharf, O., Clerbaux, C., Hadji-Lazaro, J., George, M., and Turquety, S.: FORLI radiative transfer and retrieval code for IASI, J. Quant. Spectrosc. Radiat. Transf., 113, 11, 1391–1408, 2012.

Jacob, D. J., Crawford, J. H., Maring, H., Clarke, A. D., Dibb, J. E., Emmons, L. K., Ferrare, R. A., Hostetler, C. A., Russell, P. B., Singh, H. B., Thompson, A. M., Shaw, G. E., McCauley, E., Pederson, J. R., and Fisher, J. A.: The Arctic Research of the Composition of the Troposphere from Aircraft and Satellites (ARCTAS) mission: design, execution, and first results, Atmos. Chem. Phys., 10, 5191–5212, doi:10.5194/acp-10-5191-2010, 2010.

Keim, C., Eremenko, M., Orphal, J., Dufour, G., Flaud, J.-M., Höpfner, M., Boynard, A., Clerbaux, C., Payan, S., Coheur, P.-F., Hurtmans, D., Claude, H., Dier, H., Johnson, B., Kelder, H., Kivi, R., Koide, T., López Bartolomé, M., Lambkin, K., Moore, D., Schmidlin, F. J., and Stübi, R.: Tropospheric ozone from IASI: comparison of different inversion algorithms and validation with ozone sondes in the northern middle latitudes, Atmos. Chem. Phys., 9, 9329–9347, doi:10.5194/acp-9-9329-2009, 2009.

Liu, X., Chance, K., Sioris, C. E., Spurr, R. J. D., Kurosu, T. P., Martin, R. V., and Newchurch, M. J.: Ozone profile and tropospheric ozone retrievals from the Global Ozone Monitoring Experiment: Algorithm description and validation, J. Geophys. Res., 110, D20307, doi:10.1029/2005JD006240, 2005.

McPeters, R. D., Labow, G. J., and Logan, J. A.: Ozone climatological profiles for satellite retrieval algorithms, J. Geophys. Res., 112, D05308, doi:10.1029/2005JD006823, 2007.

Mitchell Jr., J. M.: Visual range in the polar regions with particular reference to the Alaskan Arctic, J. Atmos. Terr. Phys. Special Suppl. Pt. I, 195–211, 1957.

Paris, J.-D., Ciais, P., Nédélec, P., Ramonet, M., Belan, B. D., Arshinov, M. Y., Golitsyn, G. S., Granberg, I., Stohl, A., Cayez, G., Athier, G., Boumard, F., and Cousin, J. M.: The YAK-AEROSIB transcontinental aircraft campaigns: new insights on the transport of CO_2, CO and O_3 across Siberia, Tellus B, 60, 551–568, 2008.

Paris, J.-D., Stohl, A., Nédélec, P., Arshinov, M. Yu., Panchenko, M. V., Shmargunov, V. P., Law, K. S., Belan, B. D., and Ciais, P.: Wildfire smoke in the Siberian Arctic in summer: source characterization and plume evolution from airborne measurements, Atmos. Chem. Phys., 9, 9315–9327, doi:10.5194/acp-9-9315-2009, 2009.

Parrington, M., Palmer, P. I., Henze, D. K., Tarasick, D. W., Hyer, E. J., Owen, R. C., Helmig, D., Clerbaux, C., Bowman, K. W., Deeter, M. N., Barratt, E. M., Coheur, P.-F., Hurtmans, D., Jiang, Z., George, M., and Worden, J. R.: The influence of boreal biomass burning emissions on the distribution of tropospheric ozone over North America and the North Atlantic during 2010, Atmos. Chem. Phys., 12, 2077–2098, doi:10.5194/acp-12-2077-2012, 2012.

Pommier, M., Law, K. S., Clerbaux, C., Turquety, S., Hurtmans, D., Hadji-Lazaro, J., Coheur, P.-F., Schlager, H., Ancellet, G., Paris, J.-D., Nédélec, P., Diskin, G. S., Podolske, J. R., Holloway, J. S., and Bernath, P.: IASI carbon monoxide validation over the Arctic during POLARCAT spring and summer campaigns, Atmos. Chem. Phys., 10, 10655–10678, doi:10.5194/acp-10-10655-2010, 2010.

Quennehen, B., Schwarzenboeck, A., Schmale, J., Schneider, J., Sodemann, H., Stohl, A., Ancellet, G., Crumeyrolle, S., and Law, K. S.: Physical and chemical properties of pollution aerosol particles transported from North America to Greenland as measured during the POLARCAT summer campaign, Atmos. Chem. Phys., 11, 10947–10963, doi:10.5194/acp-11-10947-2011, 2011.

Rao, N. T., Arvelius, J., Kirkwood, S., and von der Gathen, P.: Climatology of ozone in the troposphere and lower stratosphere over the european arctic, Adv. Space Res., 34, 754–758, doi:10.1016/j.asr.2003.05.055, 2004.

Real, E., Law, K. S., Weinzier, B., Fiebig, M., Petzold, A., Wild, O., Methven, J., Arnold, S., Stohl, A., Huntrieser, H., Roiger, A., Schlager, H., Stewart, D., Avery, M., Sachse, G., Browell, E., Ferrare, R., and Blake D.: Processes influencing ozone levels in Alaskan forest fire plumes during long-range transport over the North Atlantic, J. Geophys. Res., 112, D10S41, doi:10.1029/2006JD007576, 2007.

Ridley, B. A., Grahek, F. E., and Walega, J. G.: A small, high-sensitivity, medium-response ozone detector suitable for measurements from light aircraft, J. Atmos. Oceanic Technol., 9, 142–148, 1992.

Rodgers, C. D.: Inverse methods for atmospheric sounding: Theory and Practice, Series on Atmospheric, Oceanic and Planetary Physics – Vol. 2, World Scientific, Singapore, New Jersey, London, Hong Kong, 2000.

Rodgers, C. D. and Connor, B. J.: Intercomparison of remote sounding instruments, J. Geophys. Res., 108, 4116, doi:10.1029/2002JD002299, 2003.

Roiger, A., Schlager, H., Schäfler, A., Huntrieser, H., Scheibe, M., Aufmhoff, H., Cooper, O. R., Sodemann, H., Stohl, A., Burkhart, J., Lazzara, M., Schiller, C., Law, K. S., and Arnold, F.: In-situ observation of Asian pollution transported into the Arctic lowermost stratosphere, Atmos. Chem. Phys., 11, 10975–10994, doi:10.5194/acp-11-10975-2011, 2011.

Ryerson, T., Buhr, M. P., Frost, G. J., Goldan, P. D., Holloway, J. S., Hübler, G., Jobson, B. T., Kuster, W. C., McKeen, S. A., Parrish, D. D., Roberts, J. M., Sueper, D. T., Trainer, M., Williams J., and Fehsenfeld, F. C.: Emissions lifetimes and ozone formation in power plant plumes, J. Geophys. Res., 103, 22569–22583, 1998.

Scannell, C., Hurtmans, D., Boynard, A., Hadji-Lazaro, J., George, M., Delcloo, A., Tuinder, O., Coheur, P.-F., and Clerbaux, C.: Antarctic ozone hole as observed by IASI/MetOp for 2008–2010, Atmos. Meas. Tech., 5, 123–139, doi:10.5194/amt-5-123-2012, 2012.

Schlager, H., Konopka, P., Schulte, P., Schumann, U., Ziereis, H., Arnold, F., Klemm, M., Hagen, D. Whitefield, P., and Ovarlez, J.: In situ observations of air traffic emission signatures in the North Atlantic flight corridor, J. Geophys. Res., 102, 10739–10750, 1997.

Schmale, J., Schneider, J., Ancellet, G., Quennehen, B., Stohl, A., Sodemann, H., Burkhart, J. F., Hamburger, T., Arnold, S. R., Schwarzenboeck, A., Borrmann, S., and Law, K. S.: Source identification and airborne chemical characterisation of aerosol pollution from long-range transport over Greenland during POLARCAT summer campaign 2008, Atmos. Chem. Phys., 11, 10097–10123, doi:10.5194/acp-11-10097-2011, 2011.

Shindell, D. T., Chin, M., Dentener, F., Doherty, R. M., Faluvegi, G., Fiore, A. M., Hess, P., Koch, D. M., MacKenzie, I. A., Sanderson, M. G., Schultz, M. G., Schulz, M., Stevenson, D. S., Teich, H., Textor, C., Wild, O., Bergmann, D. J., Bey, I., Bian, H., Cuvelier, C., Duncan, B. N., Folberth, G., Horowitz, L. W., Jonson, J., Kaminski, J. W., Marmer, E., Park, R., Pringle, K. J., Schroeder, S., Szopa, S., Takemura, T., Zeng, G., Keating, T. J., and Zuber, A.: A multi-model assessment of pollution transport to the Arctic, Atmos. Chem. Phys., 8, 5353–5372, doi:10.5194/acp-8-5353-2008, 2008.

Sodemann, H., Pommier, M., Arnold, S. R., Monks, S. A., Stebel, K., Burkhart, J. F., Hair, J. W., Diskin, G. S., Clerbaux, C., Coheur, P.-F., Hurtmans, D., Schlager, H., Blechschmidt, A.-M., Kristjánsson, J. E., and Stohl, A.: Episodes of cross-polar transport in the Arctic troposphere during July 2008 as seen from models, satellite, and aircraft observations, Atmos. Chem. Phys., 11, 3631–3651, doi:10.5194/acp-11-3631-2011, 2011.

Thouret, V., Marenco, A., Logan, J., Nédélec, P., and Grouhel, C.: Comparisons of ozone measurements from the MOZAIC airborne program and the ozone sounding network at eight locations, J. Geophys. Res., 103, 25695–25720, 1998.

Warneke, C., Bahreini, R., Brioude, J., Brock, C. A. , de Gouw, J. A. , Fahey, D. W. , Froyd, K. D. , Holloway, J. S., Middlebrook, A., Miller, L. , Montzka, S., Murphy, D. M., Peischl, J., Ryerson, T. B., Schwarz, J. P., Spackman, J. R., and Veres, P.: Biomass burning in Siberia and Kazakhstan as an important source for haze over the Alaskan Arctic in April 2008, Geophys. Res. Lett., 36, L02813, doi:10.1029/2008GL036194, 2009.

Wespes, C., Emmons, L., Edwards, D. P., Hannigan, J., Hurtmans, D., Saunois, M., Coheur, P.-F., Clerbaux, C., Coffey, M. T., Batchelor, R. L., Lindenmaier, R., Strong, K., Weinheimer, A. J., Nowak, J. B., Ryerson, T. B., Crounse, J. D., and Wennberg, P. O.: Analysis of ozone and nitric acid in spring and summer Arctic pollution using aircraft, ground-based, satellite observations and MOZART-4 model: source attribution and partitioning, Atmos. Chem. Phys., 12, 237–259, doi:10.5194/acp-12-237-2012, 2012.

Ziemke, J. R., Joiner, J., Chandra, S., Bhartia, P. K., Vasilkov, A., Haffner, D. P., Yang, K., Schoeberl, M. R., Froidevaux, L., and Levelt, P. F.: Ozone mixing ratios inside tropical deep convective clouds from OMI satellite measurements, Atmos. Chem. Phys., 9, 573–583, doi:10.5194/acp-9-573-2009, 2009.

Zyryanov, D., Foret, G., Eremenko, M., Beekmann, M., Cammas, J.-P., D'Isidoro, M., Elbern, H., Flemming, J., Friese, E., Kioutsioutkis, I., Maurizi, A., Melas, D., Meleux, F., Menut, L., Moinat, P., Peuch, V.-H., Poupkou, A., Razinger, M., Schultz, M., Stein, O., Suttie, A. M., Valdebenito, A., Zerefos, C., Dufour, G., Bergametti, G., and Flaud, J.-M.: 3-D evaluation of tropospheric ozone simulations by an ensemble of regional Chemistry Transport Model, Atmos. Chem. Phys., 12, 3219-3240, doi:10.5194/acp-12-3219-2012, 2012.